Cell Reports

Alternative splicing and heparan sulfation converge on neurexin-1 to control glutamatergic transmission and autism-related behaviors

Graphical abstract

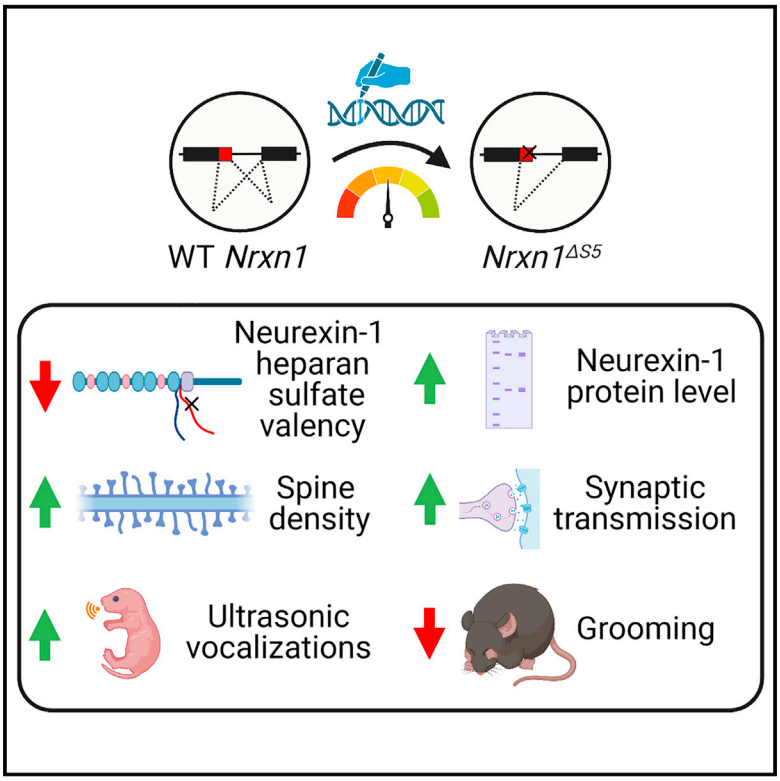

Highlights

- Nrxn1 splice insert S5 increases heparan sulfate valency and reduces protein level
- S5 does not alter Nrxn1 interaction with neuroligin or LRRTM or presynaptic induction
- Nrxn1 S5 exclusion boosts hippocampal excitatory synapse density and transmission
- Nrxn1 S5 exclusion enhances mouse pup ultrasonic vocalization and reduces grooming

Authors

Hong Lu, Long Zuo, Kyle M. Roddick, ..., Mathias Delhaye, Richard E. Brown, Ann Marie Craig

Correspondence

acraig@mail.ubc.ca

In brief

Lu et al. find that exclusion of the Nrxn1 S5 splice insert increases protein level, boosts hippocampal excitatory transmission, and shifts communication and repetitive behaviors away from the autism spectrum. Thus, *NRXN1* S5 exclusion may be a therapeutic approach toward restoring function in people with *NRXN1* haploinsufficiency and neurodevelopmental disorders.

Lu et al., 2023, Cell Reports *42*, 112714
July 25, 2023
https://doi.org/10.1016/j.celrep.2023.112714

CellPress

Cell Reports

CellPress
OPEN ACCESS

Report

Alternative splicing and heparan sulfation converge on neurexin-1 to control glutamatergic transmission and autism-related behaviors

Hong Lu,[1] Long Zuo,[1,3] Kyle M. Roddick,[2] Peng Zhang,[1,4] Shinichiro Oku,[1,5] Jessica Garden,[2] Yuan Ge,[1] Michael Bellefontaine,[2] Mathias Delhaye,[1] Richard E. Brown,[2] and Ann Marie Craig[1,6,*]

[1]Djavad Mowafaghian Centre for Brain Health and Department of Psychiatry, University of British Columbia, Vancouver, BC V6T 2B5, Canada
[2]Department of Psychology and Neuroscience, Dalhousie University, Halifax, NS B3H 4R2, Canada
[3]Present address: Ranomics, Mississauga, ON L4V 1T4, Canada
[4]Present address: Department of Neurosciences, School of Medicine, Case Western Reserve University, Cleveland, OH 44106, USA
[5]Present address: Department of Physiology and Pathophysiology, University of Manitoba, Winnipeg, MB R3E 0J9, Canada
[6]Lead contact
*Correspondence: acraig@mail.ubc.ca
https://doi.org/10.1016/j.celrep.2023.112714

SUMMARY

Neurexin synaptic organizing proteins are central to a genetic risk pathway in neuropsychiatric disorders. Neurexins also exemplify molecular diversity in the brain, with over a thousand alternatively spliced forms and further structural heterogeneity contributed by heparan sulfate glycan modification. Yet, interactions between these modes of post-transcriptional and post-translational modification have not been studied. We reveal that these regulatory modes converge on neurexin-1 splice site 5 (S5): the S5 insert increases the number of heparan sulfate chains. This is associated with reduced neurexin-1 protein level and reduced glutamatergic neurotransmitter release. Exclusion of neurexin-1 S5 in mice boosts neurotransmission without altering the AMPA/NMDA ratio and shifts communication and repetitive behavior away from phenotypes associated with autism spectrum disorders. Thus, neurexin-1 S5 acts as a synaptic rheostat to impact behavior through the intersection of RNA processing and glycobiology. These findings position *NRXN1* S5 as a potential therapeutic target to restore function in neuropsychiatric disorders.

INTRODUCTION

The specification of synaptic properties such as presynaptic neurotransmitter release probability and postsynaptic receptor composition is fundamental for brain function. Such properties are controlled by transcellular complexes of synaptic organizing proteins, which recruit components to developing synapses.[1–3] Among these, presynaptic neurexins (Nrxns) are perhaps the best studied, in part because they are genetic risk factors for human brain-based disorders.[4–6] Functionally disruptive mutations in *NRXN*s have been consistently found in autism spectrum disorders (ASDs) at the core of a synaptic pathway.[7–9] *NRXN1* is also among the strongest single-gene mutations in schizophrenia and Tourette's syndrome.[10,11] However, Nrxn regulatory mechanisms that might be harnessed for therapeutic approaches have been poorly studied.

One of the challenges and simultaneous wonders of studying Nrxns lies in their extensive heterogeneity. There are three mammalian genes, *Nrxn1–3*, each utilizing multiple promoters to generate longer α and shorter β forms and, for *Nrxn1*, a very short γ form. Nrxns undergo alternative splicing at up to six splice sites, S1–S6, giving rise to thousands of variants.[12–14] Nrxns are further modified post-translationally by a rare glycan heparan sulfate (HS).[15] In other such proteoglycans, both the number of attached glycan chains and their sulfation patterns contribute structural and functional diversity.[16–19] Nrxns are also notable for signaling through an extensive repertoire of postsynaptic ligands including neuroligins (NLs), leucine-rich repeat transmembrane proteins (LRRTMs), and glutamate receptor δ via cerebellins.[4,6,20]

Although phenotypes of complete *Nrxn1*-null mice have not yet been reported, mice lacking Nrxn1α show deficits in synaptic transmission and behavior. Nrxn1α knockout mice show reduced miniature excitatory postsynaptic current (mEPSC) frequency and reduced input-output response in the hippocampal CA1 region,[21] similar to reductions in synaptic transmission upon mutation of *NRXN1* in cultured induced human neurons.[22] Behavioral phenotypes of Nrxn1α knockout mice include reduced ultrasonic vocalization, increased grooming, altered social interactions, impaired nest building, and increased aggression of male mice.[21,23–25] Targeted mouse analyses also support the importance of both alternative splicing at Nrxn1 S4 and HS modification. Specifically, mice expressing HS-deficient Nrxn1, which reduces its interaction with NLs

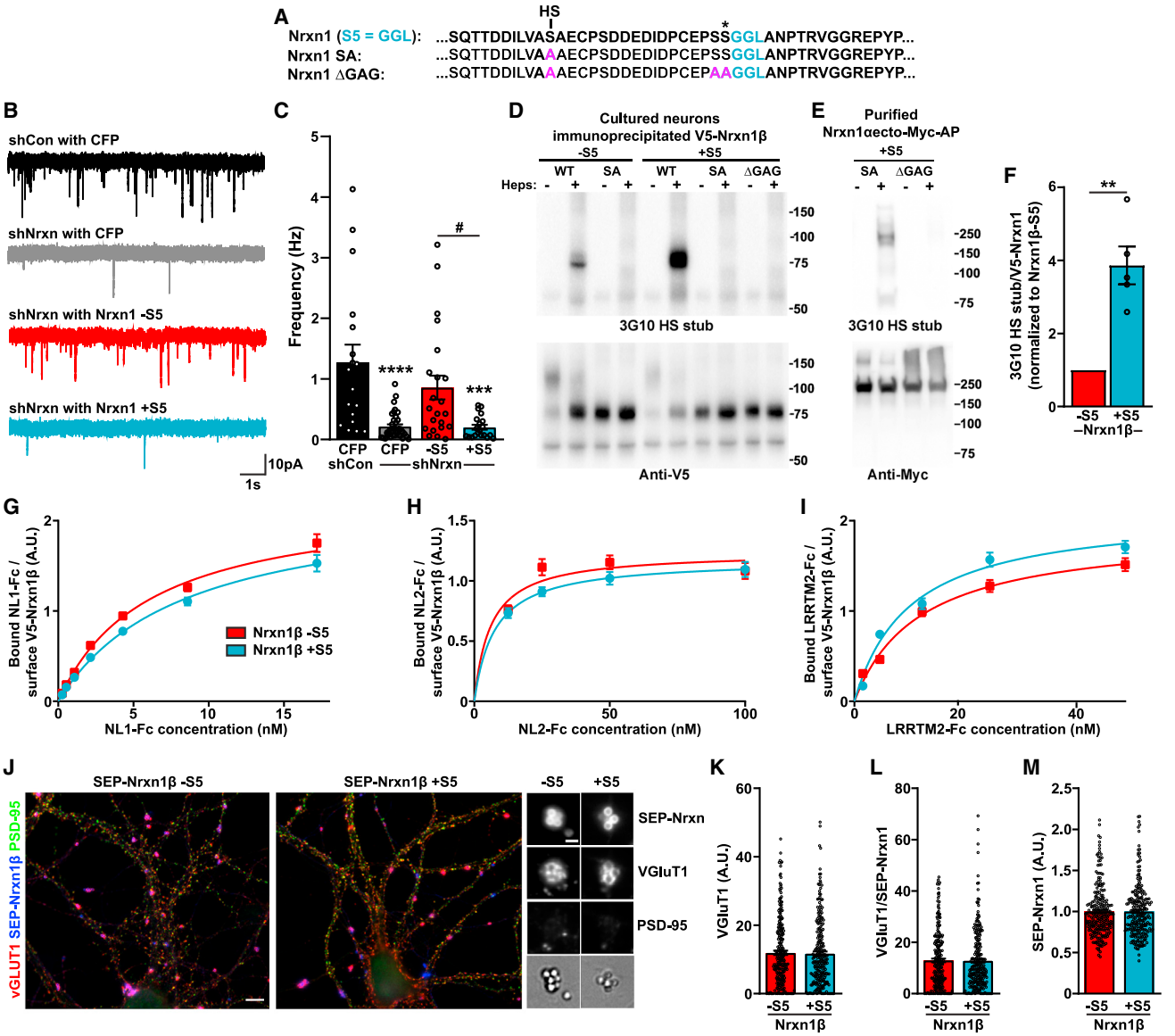

Figure 1. The Nrxn1 S5 insert reduces synaptic transmission and increases HS valency without altering ligand binding or presynaptic induction in cultured neurons

(A) Nrxn1 sequences surrounding S5 show the constitutive HS modification site, mutant sequences, and an additional HS modification site (*) detected in a Nrxn1 +S5 form.

(B and C) Excitatory transmission was impaired after Nrxn1,2,3 triple knockdown (shNrxn) and rescued by expression of RNAi-resistant Nrxn1 −S5 but not Nrxn1 +S5. $p < 0.0001$ by Kruskal-Wallis with ***$p < 0.001$ and ****$p < 0.0001$ by Dunn's post hoc test compared with control shCon with CFP; #$p < 0.05$ comparing shNrxn with Nrxn1 −S5 with shNrxn with Nrxn1 +S5; n = 18–36 cells from 3–7 independent experiments.

(D–F) The S5 insert increased HS valency of V5-Nrxn1, assessed from the ratio of 3G10/V5 signal of V5-Nrxn1β +S5 relative to −S5 (D and F; t test with Welch's correction **$p < 0.01$, n = 5). 3G10 recognizes the HS stub only after heparinase (Heps) treatment. HS modification at the * site (A) in the absence of the constitutive HS modification site was not a major modification in cultured neurons (D, comparing +S5 SA and ΔGAG mutants) but could be detected in purified concentrated Nrxn1 ectodomain (E).

(G–I) Binding of purified ligand ectodomain Fc fusion proteins was indistinguishable on the surface of immature neurons expressing V5-Nrxn1β −S5 or +S5. Scatchard analysis yielded apparent K_d (nM) values for Nrxn1 −S5 and +S5 of 6.3 and 7.8 (NL1-Fc), 6 and 7.5 (NL2-Fc), and 12.1 and 10.2 (LRRTM2-Fc) and Bmax (nM) values of 2.3 and 2.2 (NL1-Fc), 1.2 and 1.2 (NL2-Fc), and 1.9 and 2.1 (LRRTM2-Fc). All $p > 0.1$ by extra sum-of-squares F-test, $n \geq 15$ cells per concentration.

(J–M) SEP-Nrxn1β −S5 and +S5 did not differ in mediating recruitment of VGlut1 when aggregated with anti-GFP antibody-coated beads. Induced clusters were distinguished from native synapses by the absence of PSD-95 as well as the presence of a bead. SEP-Nrxn1β −S5 and +S5 mediated equal recruitment of VGlut1

(legend continued on next page)

and LRRTMs, exhibit structural presynaptic and postsynaptic deficits, impairments in presynaptic release, and reduced survival rate.[15] Forced inclusion of S4 in Nrxn1 or in all 3 Nrxns, which is required for interaction with cerebellins but blocks interaction with LRRTMs, alters the AMPA/NMDA ratio and impairs cognitive behavior.[26,27]

Among Nrxn1 splice sites, only S4 has been well studied. The function of S5, the only splice site common to all Nrxn1 isoforms α, β, and γ, is not known. The unusual, essentially invariant ~50% inclusion of the Nrxn1 S5 insert in numerous cell types[28–31] suggests an important function. Here, we uncover a surprising role of Nrxn1 S5 at the intersection of RNA processing and glycobiology, acting as a rheostat for synaptic transmission to impact mouse behavior.

RESULTS

Nrxn1 S5 insertion reduces synaptic function and increases HS valency in cultured hippocampal neurons

As an initial test for the function of Nrxn1 S5, we used a molecular replacement strategy in cultured hippocampal neurons. We knocked down all Nrxns[15] and rescued with a mixture of RNAi-resistant Nrxn1α and -1β with or without the 3-amino acid S5 splice insert. Nrxn knockdown reduced mEPSC frequency (Figures 1B, 1C, and S1B), consistent with our previous observations and with deficits in α-Nrxn- or β-Nrxn-deficient neurons.[15,32,33] Despite a transfection efficiency of ~60%, this reduction was fully rescued by Nrxn1 lacking the S5 insert (Nrxn1 −S5), but no rescue was observed by Nrxn1 containing the S5 insert (Nrxn1 +S5) (Figures 1B, 1C, and S1B). Thus, inclusion of Nrxn1 S5 reduces synaptic function.

In considering the proximity of S5 to the HS modification site on Nrxn1 (Figure 1A) and previous data suggesting that Nrxns are partially modified with HS,[15] we wondered whether S5 might regulate the extent of Nrxn1 HS modification. To address this, we used a monoclonal antibody, 3G10, which recognizes the exposed stub on HS chains cleaved by heparinase.[34] Indeed, we found that the 3G10 HS stub/V5-Nrxn1 ratio for heparinase-treated V5-Nrxn1 immunoprecipitated from transfected cultured neurons was 3.9-fold higher for Nrxn1 +S5 than for −S5, indicating an increase in the number of HS chains, i.e., increased HS valency (Figures 1D–1F). The S5 insert creates a second potential HS modification site at the adjacent serine (S* in Figure 1A). In the absence of the constitutive HS modification site, this second serine was not a major modification site in cultured neurons but was detected in an HS-modified form in a purified concentrated Nrxn1 +S5 ectodomain and was the only additional HS modification site detected (Figures 1D and 1E). Taken together, these data suggest that S5 enhances HS valency by conferring a distinct HS attachment site that acts in synergy with the constitutive site to post-translationally modify Nrxn1. Such synergy is consistent with cooperativity displayed for HS modification at nearby sites on other proteoglycans.[35]

Nrxn1 S5 regulates protein level but not binding to canonical ligands or presynaptic induction

As the constitutive HS modification participates in Nrxn interaction with canonical ligands NLs and LRRTMs[15] and S5 alters HS valency, we tested whether S5 affects Nrxn1 interaction with these ligands. We used a neuron-based binding assay similar to those used previously[15,36] for the two major ligands of Nrxn1 localized at excitatory hippocampal synapses, NL1 and LRRTM2, and the major one localized at inhibitory hippocampal synapses, NL2. Binding affinities of the three ligand ectodomain Fc fusions to V5-Nrxn1β expressed on cultured hippocampal neurons were not affected by the presence or absence of S5 (Figures 1G–1I, S1E, and S1F).

We next tested whether the ability of Nrxn1 to mediate presynaptic differentiation is affected by S5. Based on the previous finding that clustering of β-Nrxn on axons triggers the recruitment of synaptic vesicles,[37] we used anti-GFP antibody-coated beads to cluster superecliptic pHluorin (SEP)-tagged Nrxn1β expressed in cultured hippocampal neurons. Clustering of SEP-Nrxn1β, but not negative control YFP-MDGA1, robustly triggered recruitment of vesicular glutamate transporter 1 (VGlut1; Figures 1J–1M and S1G). However, there was no difference in the extent of VGlut1 recruitment to bead-induced clusters of SEP-Nrxn1β −S5 versus +S5, assessed by VGlut1 or the VGlut1/SEP-Nrxn1 ratio per bead aggregate, comparing beads of equal SEP-Nrxn. Furthermore, the active zone proteins bassoon and ELKS were also robustly recruited by SEP-Nrxn1β indistinguishably between the −S5 and +S5 forms (Figures S1H–S1O). These results suggest that Nrxn1 S5 does not regulate presynaptic induction activity or postsynaptic ligand interactions.

The possibilities remain that differential rescue of synaptic function by Nrxn1 −S5 versus Nrxn1 +S5 may be due to a difference in Nrxn surface trafficking or protein levels. We transfected cultured hippocampal neurons with YFP-P2A-V5-Nrxn1β −S5 or +S5, using the P2A linker[38] to express initial equimolar YFP and V5-Nrxn1, and immunostained for surface and intracellular recombinant Nrxn. Neurons expressing the −S5 splice form showed higher levels of both surface and intracellular V5-Nrxn relative to YFP than the +S5 form (Figures 2A–2D and S1A), with no change in the efficiency of surface trafficking. To assess whether these effects may be related to the change in HS valency, we tested Nrxn1 +S5 AAGGL, leaving the S5 insert intact but mutating the prior serine residues to remove the additional HS modification site conferred by S5. Nrxn1 +S5 AAGGL showed surface and total levels distinct from Nrxn1 +S5 and indistinguishable from Nrxn1 −S5 (Figure 2A–2D and S1A). These results suggest that the increase in HS valency induced by the S5 insert mediates the reduction in steady-state protein level of Nrxn1.

immunofluorescence mean intensity per bead aggregate (K, normalized to the VGlut1 associated with beads clustering negative control YFP-MDGA1, images in Figure S1G, Mann Whitney test $p > 0.1$, n = 244 bead aggregates each from 3 independent experiments) and VGlut1/SEP-Nrxn1 ratio per bead aggregate (L, $p > 0.1$). Bead aggregates analyzed did not differ in SEP-Nrxn1 (M, $p > 0.1$). Scale bars: 10 (J, left) and 2 μm (J, right).
All data are reported as mean ± SEM. See also Figure S1.

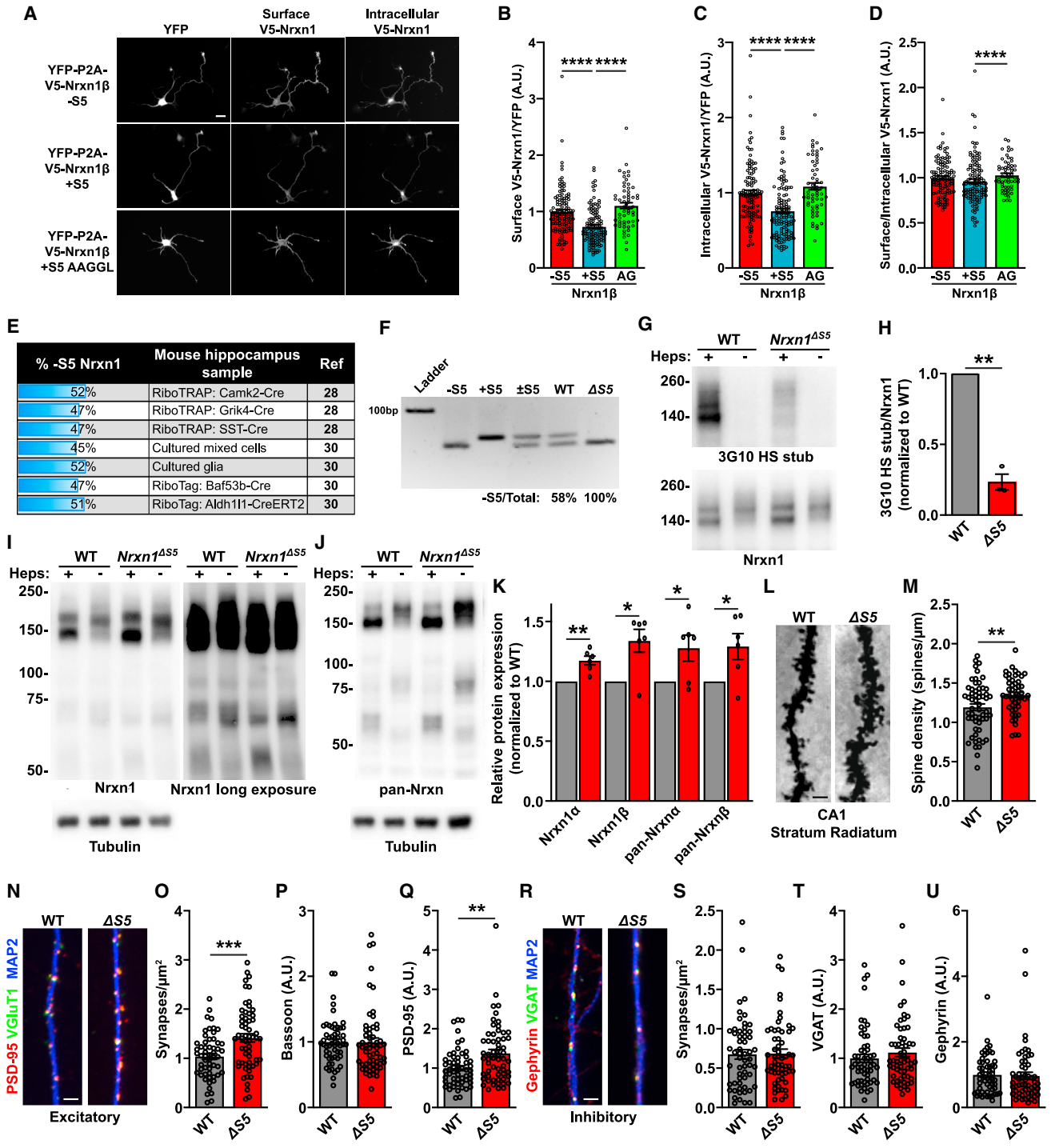

Figure 2. Nrxn1 S5 exclusion reduces HS modification and elevates protein level and excitatory synapse numbers

(A–D) V5-Nrxn1β −S5 and V5-Nrxn1β +S5 AAGGL (AG) showed greater surface and intracellular expression than V5-Nrxn1β +S5, assessed from the V5-Nrxn1 to YFP ratio from stoichiometric coexpression of YFP and Nrxn1 using the P2A linker. (B and C) $p < 0.0001$ by Kruskal-Wallis with ****$p < 0.0001$ by Dunn's post hoc test. (D) $p < 0.05$ by Kruskal-Wallis with *$p < 0.05$ by Dunn's post hoc test. n = 59–122 neurons each from 3–6 independent experiments.

(E) Previous studies indicate a Nrxn1 −S5:+S5 ratio of ~1:1 across multiple hippocampal samples.

(F) RT-PCR of WT and *Nrxn1*$^{\Delta S5}$ whole-brain mRNA with primers flanking S5. *Nrxn1*$^{\Delta S5}$ shows complete conversion of Nrxn1 to the −S5 isoform, while in WT, 58% is −S5. Recombinant plasmids encoding Nrxn1 −S5, Nrxn1 +S5, and an equimolar mixture were also run as PCR templates.

(legend continued on next page)

Exclusion of Nrxn1 S5 does not affect mouse survival or gross brain morphology but reduces Nrxn1 HS valency and increases protein level *in vivo*

Typically, Nrxn alternatively spliced exon inclusion rates vary among brain regions and cell types[39] as for most alternative splicing events. In sharp contrast, Nrxn1 S5 exhibits a ~1:1 −S5:+S5 splice program that is pervasive across multiple brain regions, including the cortex, hippocampus, and cerebellum, as well as individual cell types (Figure 2E; Table S1). Interestingly, this ~50% inclusion of *NRXN1* S5 also translates to human induced neurons.[29] Such tight unvarying regulation supports a physiological importance of Nrxn1 S5 splicing.

To examine the function of Nrxn1 S5 *in vivo*, we generated a CRISPR knockin mouse (*Nrxn1*$^{\Delta S5}$) with mutations at the second splice donor site for S5 to convert all Nrxn1 +S5 to −S5 forms (Figure S2A). RT-PCR of whole brain confirmed complete conversion from Nrxn1 +S5 to −S5 in the mutant and reproduced the ~1:1 ratio of Nrxn1 −S5:+S5 in wild-type (WT) mice (Figure 2F). Neither litter size nor survival rate was affected, although the S5 conversion resulted in mild reductions in body weight (Figures S2B, S2C, S2F, and S2G). The mRNA levels of Nrxn1 as well as other Nrxns and various synaptic components were not significantly altered in *Nrxn1*$^{\Delta S5}$ mice, and there was no obvious difference in gross brain morphology (Figures S2D and S2E).

We next determined whether the effects of Nrxn1 S5 on HS valency and Nrxn1 protein level seen in cultured neurons also occurred *in vivo*. HS chain valency, measured as the 3G10 HS stub/Nrxn1 ratio in Nrxn1 immunoprecipitated from whole-brain crude synaptosomes, was reduced 4.3-fold in *Nrxn1*$^{\Delta S5}$ mice relative to WT (Figures 2G and 2H). A significant increase in Nrxnα and -β protein levels was also seen by immunoblotting with either Nrxn1-specific or pan-Nrxn antibodies (Figures 2I–2K). These results indicate that S5 insert functions to increase Nrxn1 HS valency and reduce Nrxn1 protein levels *in vivo* and suggest that the highly regulated ratio of Nrxn1 −S5:+S5 may serve to maintain these at an optimal balance across synapses.

Nrxn1 S5 exclusion increases excitatory, but not inhibitory, synapse density

Gene dosage effects of *NRXN1* have been suggested based on clinical phenotypes of mono- and biallelic mutations found in patients with neuropsychiatric disorders.[9] This possibility, together with our finding of increased Nrxn1 protein levels in *Nrxn1*$^{\Delta S5}$ mice, prompted us to probe for synaptic and functional consequences. Nrxn1 is broadly expressed, including throughout the hippocampal formation. We first assessed synapses morphologically using Golgi staining and counting dendritic spines in the hippocampal CA1 *stratum radiatum*, where >90% of excitatory synapses form on spines.[40] Spine density was significantly increased in *Nrxn1*$^{\Delta S5}$ dendrites relative to WT (Figures 2L and 2M). Using an independent approach, an increase was found in the number of apposed clusters of bassoon and excitatory postsynaptic scaffold PSD-95 in hippocampal neurons cultured from *Nrxn1*$^{\Delta S5}$ mice (Figures 2N–2Q). In the same cultures, there was no genotype difference in the number of apposed clusters of vesicular GABA transporter (VGAT) and inhibitory scaffold gephyrin (Figures 2R–2U). There was no difference in the amount of gephyrin, VGAT, or bassoon detected per synapse, but there was an increase in PSD-95. Thus, *Nrxn1*$^{\Delta S5}$ hippocampal neurons relative to WT showed an increase in spine density, excitatory synapse density, and PSD-95 content, with no changes in inhibitory synapses.

Nrxn1 S5 exclusion boosts excitatory transmission and presynaptic neurotransmitter release

As an initial functional test, we assessed spontaneous synaptic transmission. mEPSCs recorded from CA1 pyramidal neurons in slice showed a significant ~2-fold increase in frequency in *Nrxn1*$^{\Delta S5}$ male and female mice relative to WT (Figures 3A–3J). An increase in mEPSC amplitude was also seen in males. Given the ubiquitous ~1:1 ratio of Nrxn1 −S5:+S5, we wondered whether this boost in synaptic function extends to other excitatory synapses in the hippocampus. mEPSCs recorded from CA3 neurons also showed a significant ~2-fold increase in frequency in *Nrxn1*$^{\Delta S5}$ male and female mice, with no significant difference in mEPSC amplitude (Figures S3A–S3J). No differences in frequency or amplitude were seen for miniature neurotransmission at inhibitory synapses on CA1 pyramidal neurons (Figures 3K–3O). Thus, Nrxn1 S5 exclusion boosts spontaneous transmission at two distinct hippocampal excitatory synapses but not at hippocampal inhibitory synapses.

To further assess the mechanism of increased excitatory synaptic transmission at CA1 synapses, we used males, as the S5 exclusion effects were more robust in males than females. Multiple assays of evoked transmission at Schaffer collateral-CA1 synapses were used. EPSC input-output curves were enhanced for AMPA and NMDA components (Figures 3P–3U), indicating increases in evoked as well as spontaneous transmission in *Nrxn1*$^{\Delta S5}$ mice. These changes in transmission could reflect, in

(G and H) *Nrxn1*$^{\Delta S5}$ mice exhibit a 4.3-fold reduction in Nrxn1 HS valency, measured as the 3G10 HS stub/Nrxn1 ratio and normalized to WT. Whole-brain crude synaptosomal fractions were immunoprecipitated with Nrxn1 antibody, treated as indicated with Heps to expose the 3G10 HS stub epitope, and immunoblotted. t test with Welch's correction **$p < 0.01$, n = 3 mice each.

(I–K) Nrxn protein levels are elevated in *Nrxn1*$^{\Delta S5}$ mice compared with WT. Nrxn1 (I) and pan-Nrxn1,2,3 (J) levels were estimated from crude synaptosomal fractions treated with Heps to condense the bands and signals normalized to the tubulin loading control. Long exposure times were used to visualize Nrxn1β. t test with Holm-Sidak correction, **$p < 0.01$, *$p < 0.05$, n = 6 mice each (K).

(L and M) Spine numbers on CA1 pyramidal cells in *stratum radiatum* were elevated after exclusion of Nrxn1 S5. (M) **$p < 0.01$ by t test with Welch's correction, n = 57 for WT and n = 49 dendrites for *Nrxn1*$^{\Delta S5}$ from 4–5 mice each.

(N–U) Cultured *Nrxn1*$^{\Delta S5}$ hippocampal neurons exhibited an increase in excitatory synapse numbers and PSD-95 levels, while inhibitory synapse density was unaltered. (O) ***$p < 0.001$ by t test with Welch's correction; (P) Mann Whitney test $p > 0.1$; (Q) **$p < 0.01$ by Mann Whitney test, n = 56–59 dendrites each from 3 independent experiments. (S–U) Mann Whitney test $p > 0.1$, n = 57–58 dendrites each from 3 independent experiments.

Scale bars: 20 (A) and 2.5 μm (L, N, and R).

All data are reported as mean ± SEM. See also Figures S1 and S2 and Table S1.

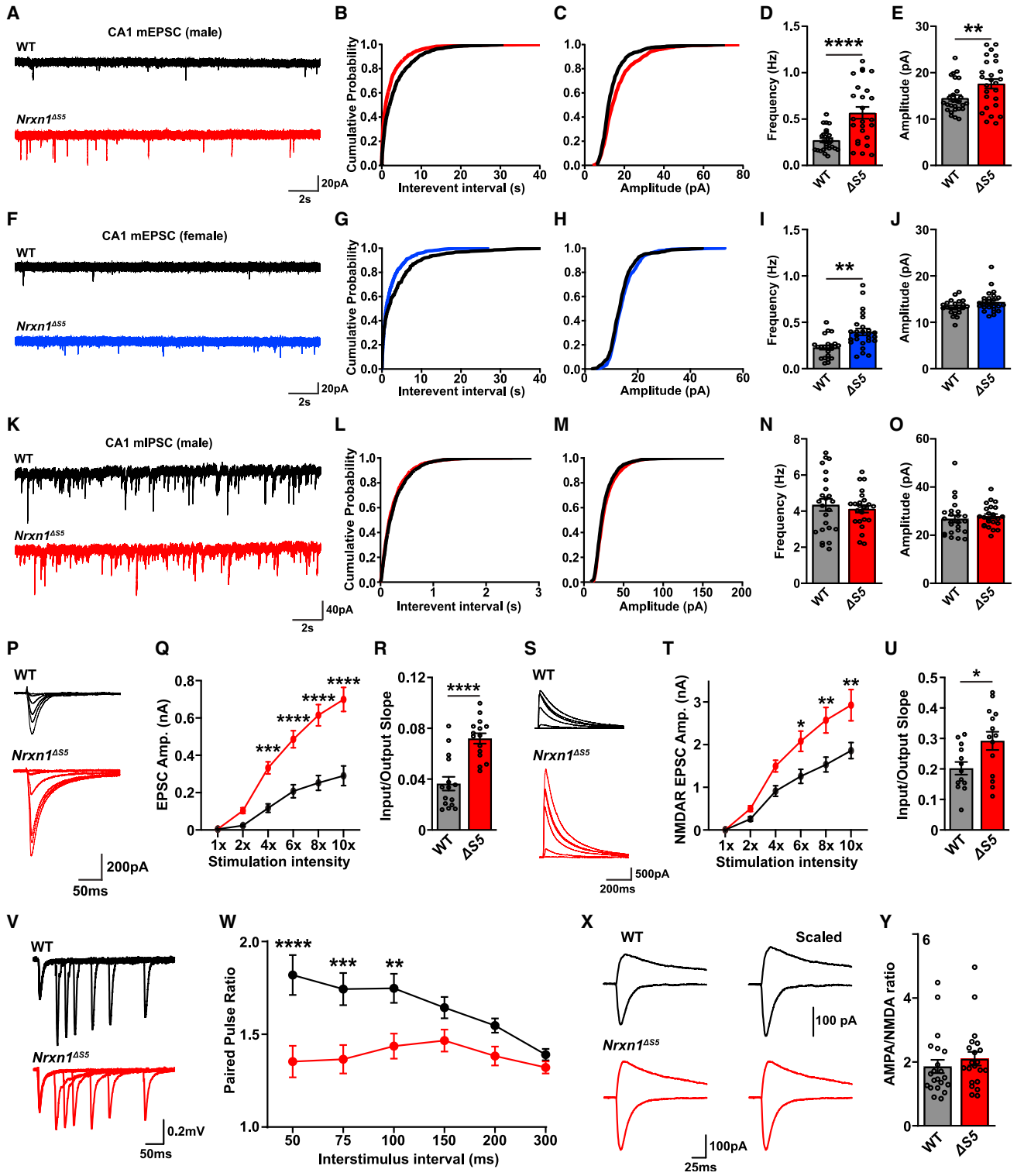

Figure 3. Nrxn1 S5 exclusion boosts excitatory synaptic transmission and probability of release at hippocampal CA3-CA1 synapses

(A–J) Exclusion of S5 boosts excitatory synaptic transmission in *Nrxn1*$^{\Delta S5}$ mice. mEPSC frequency was 2.1-fold higher in male and 1.7-fold higher in female *Nrxn1*$^{\Delta S5}$ CA1 pyramidal cells compared with WT. (D and I) Two-way ANOVA genotype $p < 0.0001$, sex $p < 0.05$ with ****$p < 0.0001$, **$p < 0.01$ by Sidak post hoc test, n = 23–26 cells from 3–5 mice each. (B and G) $p < 0.0001$ by Kolmogorov-Smirnov test. (E and J) mEPSC amplitude was significantly increased in male, but not female, Nrxn1$^{\Delta S5}$ CA1 pyramidal cells, two-way ANOVA genotype $p < 0.01$, sex $p < 0.01$ with **$p < 0.01$ by Sidak post hoc test. (C and H) Kolmogorov-Smirnov test $p < 0.001$ male and $p > 0.1$ female.

(legend continued on next page)

part, the increase in excitatory synapse density, but there could also be changes in transmitter release. Indeed, paired-pulse ratios were reduced (Figures 3V and 3W), suggesting an increased probability of transmitter release in *Nrxn1*$^{\Delta S5}$ mice. The response to stimulus trains was also increased at *Nrxn1*$^{\Delta S5}$ synapses (Figures S3K–S3O). For these synapses that have low release probability, these measures could reflect changes in the readily releasable pool and/or in the probability of transmitter release.[41] In contrast to these presynaptic alterations, and in contrast to the effect of altering Nrxn1 S4,[26] there was no difference in the evoked AMPA/NMDA ratio in *Nrxn1*$^{\Delta S5}$ slices (Figures 3X and 3Y). This finding is consistent with the lack of effect of Nrxn1 S5 on interaction with NL1 and LRRTM2 (Figure 1), which link to NMDA and AMPA receptors, respectively.[42–44] Taken together, our findings reveal a boost in presynaptic function with no evidence for postsynaptic receptor changes resulting from Nrxn1 S5 exclusion.

Nrxn1 S5 exclusion alters ultrasonic vocalization, object recognition, and grooming behavior

To understand the consequences for the organism after Nrxn1 S5 exclusion, we assessed a range of developmental behaviors, including behaviors related to ASD. *Nrxn1*$^{\Delta S5}$ pups did not differ from WT in the age at which they reached a series of neurodevelopmental reflex milestones except a short delay in eye and ear opening in females (Figures S4A and S4B). Communication problems have long been recognized as a core feature of ASD, and thus we studied mouse ultrasonic vocalization (USV). *Nrxn1*$^{\Delta S5}$ pups differed from WT in USVs during maternal isolation. The number of calls was the same for both genotypes, but the mean power of calls by both male and female *Nrxn1*$^{\Delta S5}$ pups was greater than for WT (Figures S4C, S4D, 4A, and 4C). The nature of the calls also differed as assessed from the mean slope of frequency/time (Figures 4B and 4D).

As a test of cognitive function, mice were assessed in a novel object recognition task. Relative to WT, male *Nrxn1*$^{\Delta S5}$ mice showed increased recognition of the novel over the familiar object, while females showed no genotype difference (Figures 4E, 4F, 4J, and 4K). Thus, despite a slightly lower body weight, the behavior of male *Nrxn1*$^{\Delta S5}$ pups was enhanced relative to WT in both novel object recognition and USV assays.

Another core feature of ASD is restricted, repetitive, or stereotyped patterns of behaviors, for which a related behavior in mice is grooming. Relative to WT, *Nrxn1*$^{\Delta S5}$ mice showed a decrease in total duration of grooming (Figures 4G–4I and 4L–4N). In males, this was associated with a reduced number of grooming bouts, while in females there was a reduction in mean bout duration. Thus, in multiple measures, *Nrxn1*$^{\Delta S5}$ mice showed reduced grooming compared with WT mice.

DISCUSSION

Since Nrxns were first discovered 30 years ago, much of the effort invested into understanding how their functions in specifying synaptic properties are regulated has been directed toward splice site 4. In comparison, the biological significance of the other five Nrxn splice sites or of glycan modification or how these modes may interact have received little attention. Here, we show that Nrxn1 S5 controls HS chain valency, steady-state protein level, and excitatory synapse function. Mice with all Nrxn1 converted to the −S5 form are endowed with increases in hippocampal excitatory synapse density, spontaneous and evoked transmission, and presynaptic release probability, with no changes detected at inhibitory synapses. Behaviorally, enhanced USV power, enhanced novel object recognition, and reduced grooming place *Nrxn1*$^{\Delta S5}$ mice in the opposite spectrum from *Nrxn1* knockout lines and other ASD models.

We report an unusual convergence of RNA splicing and glycobiology, with Nrxn1 S5 alternative splicing regulating proteoglycan HS valency. An interesting parallel occurs in a Nrxn ligand: the inclusion of splice site A1 on NL1 confers increased HS binding and enhances synaptic transmission.[36] Unlike splice site 4, which is homologous among Nrxn1–3, S5 is highly divergent. Critical functions of large inserts at the complex Nrxn3 S5 splice site have been identified in binding C1ql2/3 and recruiting kainate receptors[45] or in conferring GPI anchoring for proper function of dendrite-targeting interneuron synapses.[46] We identified a distinct function for S5 in Nrxn1, where an insert of only 3 amino acids increases HS valency and suppresses hippocampal excitatory synapses. This finding complements other studies showing modes of regulating the extent of Nrxn HS modification by *cis*-binding partners CA10 and FAM19A.[47,48] While a complete lack of HS on Nrxn1 (ΔGAG with 3 serine mutations as in Figure 1) leads to synaptic impairments and reduced mouse survival,[15] here we show that past a certain point, increased HS modification is not associated with maximal synaptic function. Despite having reduced Nrxn1 HS modification, *Nrxn1*$^{\Delta S5}$ mice exhibit a 2-fold increase in synaptic transmission compared with WT mice. The increased function by exclusion of S5 is linked to increased Nrxn1 protein levels, suggesting more Nrxn1 present at the synapse. Given the role of Nrxns in coupling presynaptic calcium channels to release,[32,49,50] it is likely that more Nrxn1

(K–O) Inhibitory synaptic transmission is largely unaffected in male *Nrxn1*$^{\Delta S5}$ mice.

(P–R) Evoked excitatory transmission at CA3-CA1 synapses was bolstered by S5 exclusion. (Q) Two-way ANOVA genotype $p < 0.0001$, stimulation intensity $p < 0.0001$, genotype stimulation intensity interaction $p < 0.0001$ with ****$p < 0.0001$, ***$p < 0.001$ by Sidak post hoc test. (R) t test with Welch's correction ****$p < 0.0001$. n = 15 cells from 4 mice each.

(S–U) Nrxn1 S5 exclusion increases NMDAR-mediated synaptic responses at CA3-CA1 synapses. (T) Two-way ANOVA genotype $p < 0.0001$, stimulation intensity $p < 0.0001$, genotype stimulation intensity interaction $p < 0.05$ with **$p < 0.01$, *$p < 0.05$ by Sidak post hoc test. (U) t test with Welch's correction *$p < 0.05$. n = 13–14 cells from 4 mice each.

(V and W) Paired-pulse ratios of hippocampal CA3-CA1 synapses are reduced in *Nrxn1*$^{\Delta S5}$ mice compared with WT. Genotype $p < 0.01$ by two-way repeated measures (RM) ANOVA with ****$p < 0.0001$, ***$p < 0.001$, and **$p < 0.01$ by Sidak post hoc test, n = 17–18 cells from 5–6 mice each.

(X and Y) AMPA/NMDA ratio is not significantly altered at CA3-CA1 synapses of *Nrxn1*$^{\Delta S5}$ mice compared with WT. (X) In the representative traces at right, the WT traces were scaled up. (Y) Mann-Whitney test $p > 0.1$, n = 21 cells from 7–11 mice each.

All data are reported as mean ± SEM. See also Figure S3.

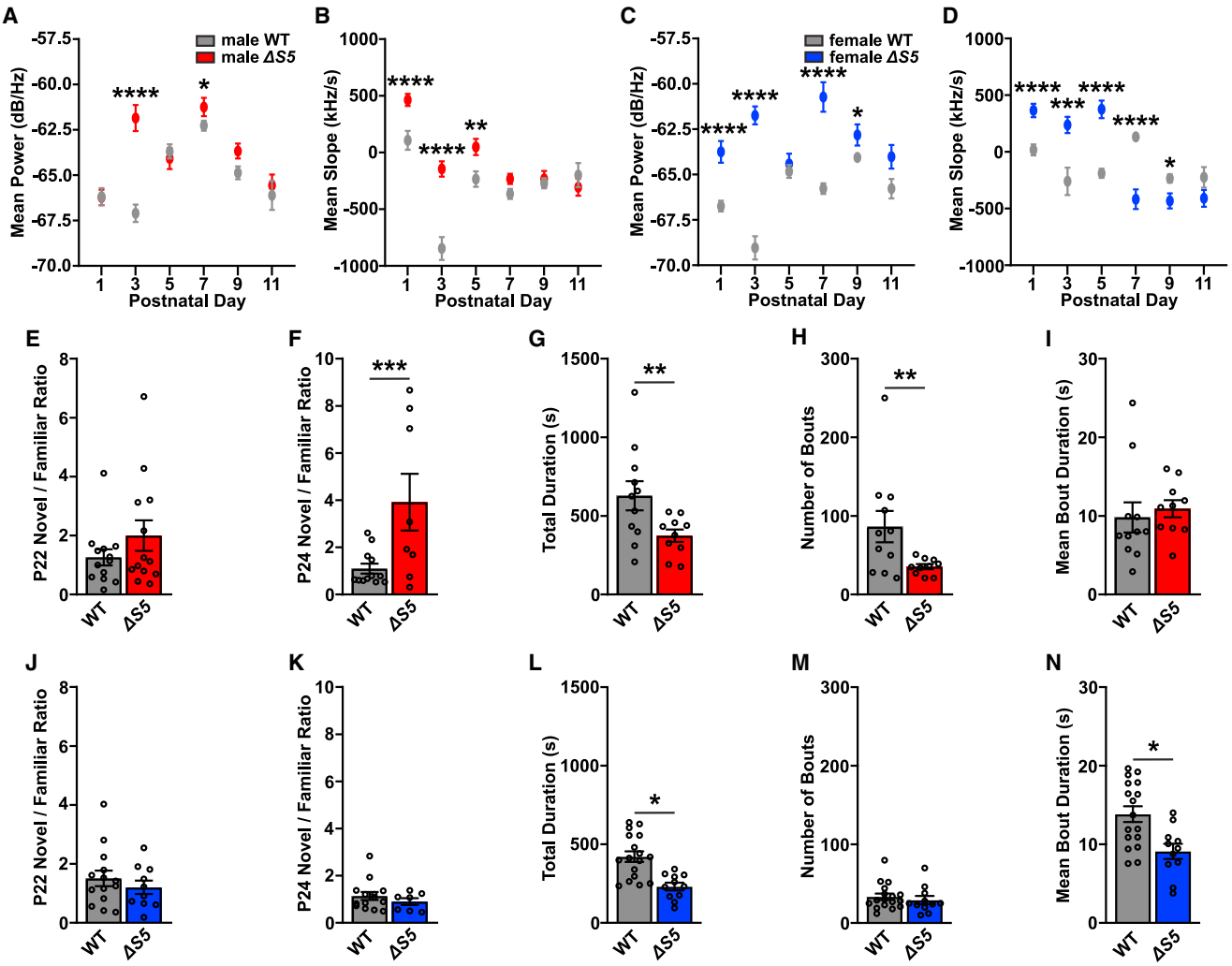

Figure 4. Nrxn1 S5 exclusion alters vocalization and grooming behavior

(A–D) Quantitative analyses of isolation-induced ultrasonic vocalizations reveal increased mean call power and slope in both male and female *Nrxn1*$^{\Delta S5}$ pups. Three-way ANOVA for power: genotype $p < 0.0001$, sex $p < 0.001$, age $p < 0.0001$, genotype sex interaction $p < 0.0001$, and genotype age interaction $p < 0.0001$; three-way ANOVA for slope: genotype $p < 0.0001$, sex $p < 0.0001$, age $p < 0.0001$, genotype sex interaction $p < 0.05$, and genotype age interaction $p < 0.0001$ with ****$p < 0.0001$, ***$p < 0.001$, **$p < 0.01$, and *$p < 0.05$ by Sidak post hoc test, n = 82–876 calls from 8–12 mice each.

(E, F, J, and K) Male *Nrxn1*$^{\Delta S5}$ mice showed improved performance in the novel object recognition task. At postnatal day 22 (P22), there was no significant difference among groups; two-way ANOVA all $p > 0.1$. At P24, two-way ANOVA genotype $p < 0.05$, sex $p < 0.01$, genotype sex interaction $p < 0.01$ with ***$p < 0.001$ by Sidak post hoc test, n = 8–14 mice each.

(G–I and L–N) *Nrxn1*$^{\Delta S5}$ male and female mice exhibited reduced grooming behavior. Two-way ANOVA for total duration: genotype $p < 0.001$, sex $p < 0.01$, and genotype sex interaction $p > 0.1$; two-way ANOVA for number of bouts: genotype $p < 0.01$, sex $p < 0.01$, and genotype sex interaction $p < 0.05$; two-way ANOVA for mean bout duration: genotype and sex $p > 0.1$, and genotype sex interaction $p < 0.05$. **$p < 0.01$ and *$p < 0.05$ by Sidak post hoc test, n = 10–17 mice each. All data are reported as mean ± SEM. See also Figure S4.

at the synapse could be the driving force behind the increased presynaptic release in *Nrxn1*$^{\Delta S5}$ mice through elevated calcium channel coupling. The lack of effect of Nrxn1 S5 and the associated change in HS valency on binding to NLs is compatible with the structure of the NL1-Nrxn1β complex (PDB: 3VKF) and the observation that one HS chain on one of the two bound Nrxns is sufficient to fill the HS-binding site at the NL1 dimer interface.[15] Altogether, there seems to be a sweet spot of HS valency on Nrxn1 for maximal synaptic function, achieved by Nrxn1 −S5.

Behaviorally, *Nrxn1*$^{\Delta S5}$ mice display some phenotypes opposite to those observed in *Nrxn1* knockout animals and to behaviors implicated in ASD. *Nrxn1α* knockout mice exhibited an increased number of bouts and total duration of grooming[21] (but see also Grayton et al.[24]), in direct contrast to the *Nrxn1*$^{\Delta S5}$ mice. *Nrxn1α* knockout mice as well as several *Nlgn* and *Shank* mouse models of ASD show deficits in USV,[23,51,52] in contrast to the increased call power in *Nrxn1*$^{\Delta S5}$ mice. Performance in the novel object recognition task was indistinguishable in *Nrxn1α*

knockout mice but enhanced in *Nrxn1*$^{\Delta S5}$ male mice. Altogether, Nrxn1 S5 exclusion enhanced performance in a cognitive test and shifted behavior away from the autism spectrum in assays related to communication and repetitive behavior.

Based on this behavioral phenotype and the enhanced excitatory transmission in *Nrxn1*$^{\Delta S5}$ mice, which directly contrasts the reduced transmission seen in *Nrxn1*α knockout mice and *NRXN1*$^{+/-}$ induced human neurons,[21,22] we suggest that *NRXN1* S5 may be a suitable therapeutic target. Although the S5 region is included in some disorder-associated *NRXN1* deletions, it is not a specific disease focus.[9,29] Thus, we do not propose to correct the mutant *NRXN1* allele but rather to alter S5 splicing of the remaining unaffected allele to partially restore Nrxn1 protein levels and function. Specifically, in cases of heterozygous *NRXN1* mutations in ASD and schizophrenia, exclusion of S5 at the remaining WT *NRXN1* allele may serve as a therapeutic avenue to boost function of the remaining Nrxn1 and alleviate deficits. The two Nrxn1 S5 isoforms did not show differences in presynaptic recruitment of VGlut1, bassoon, or ELKS or in binding affinities to canonical postsynaptic ligands, and the AMPA/NMDA ratio was unchanged in *Nrxn1*$^{\Delta S5}$ mice. Therefore, exclusion of S5 as a rescue strategy may be a path to elevating Nrxn level and function while maintaining the physiological balance of Nrxn interactors and postsynaptic receptors. Furthermore, the ~1:1 ratio of Nrxn1 −S5:+S5 observed across WT neuron types provides a wide dynamic range for functional change. Our findings also raise the possibility of utilizing Nrxn1 S5 conversion to mitigate neurological deficits associated with synaptic impairment brought on by mutations outside of *NRXN1* itself or even in neurodegenerative disorders.

Limitations of the study

First, while our data suggest that Nrxn1 S5 acts through altering HS valency and protein level, we cannot rule out a role for additional molecular interactions. Further studies will be required to determine whether S5, or HS, regulates Nrxn1 binding to cerebellins or novel synaptic partners. Second, we focused on hippocampal CA1 and CA3 synapses and a subset of behaviors. It will be important to determine brain wide which circuits are affected by Nrxn1 S5 splicing to assess a broader range of behaviors and to relate specific circuit changes to behavior. Third, further tests of the idea that Nrxn1 S5 exon skipping may restore function in cases of Nrxn1 haploinsufficiency are warranted in animal models and human cells. In a broader context, the potential for Nrxn1 S5 exon skipping to alleviate deficits in synaptic transmission in more diverse situations will depend on the affected molecular pathways and circuits.

STAR★METHODS

Detailed methods are provided in the online version of this paper and include the following:

- KEY RESOURCES TABLE
- RESOURCE AVAILABILITY
  - Lead contact
  - Materials availability
  - Data and code availability
- EXPERIMENTAL MODEL AND STUDY PARTICIPANT DETAILS
  - Mice
  - Primary neuron culture
  - Cell line culture
- METHOD DETAILS
  - Plasmid constructs
  - Neurexin molecular replacement in culture
  - Neuron culture immunoprecipitation
  - Ectodomain fusion protein production
  - Immunocytochemistry
  - Ligand binding assays
  - Bead induction assays
  - RT-PCR and qPCR
  - DAPI staining for gross brain morphology
  - Preparation of crude synaptosomal fraction
  - Immunoprecipitation and immunoblotting
  - Golgi staining and spine counts
  - Hippocampal slice electrophysiology
  - Behavior
  - Neurodevelopmental milestones
  - Novel object recognition
  - Ultrasonic vocalization
  - Grooming
- QUANTIFICATION AND STATISTICAL ANALYSIS

SUPPLEMENTAL INFORMATION

Supplemental information can be found online at https://doi.org/10.1016/j.celrep.2023.112714.

ACKNOWLEDGMENTS

We thank Xiling Zhou and Nazarine Fernandes for excellent technical assistance. Funding was provided by Simons Foundation Autism Research Initiative SFARI 608066 to A.M.C. and R.E.B., Canadian Institutes of Health Research FDN-143206 and PJT-183943 to A.M.C., Natural Sciences and Engineering Research Council of Canada A7441 to R.E.B, a Vanier Canada Graduate Scholarship to H.L., and a Brain Canada's Shireen and Edna Marcus Excellence Award to H.L.

AUTHOR CONTRIBUTIONS

The overall project was designed by H.L., P.Z., R.E.B., and A.M.C. Experiments were designed and performed and data analyzed by H.L., L.Z., P.Z., S.O., Y.G., and M.D. under the oversight of A.M.C. and by K.M.R., J.G., and M.B. under the oversight of R.E.B. for the behavioral analyses. The manuscript was written by H.L. and A.M.C. with input from all authors.

DECLARATION OF INTERESTS

The authors declare no competing interests.

Received: July 22, 2022
Revised: April 16, 2023
Accepted: June 13, 2023

REFERENCES

1. Südhof, T.C. (2018). Towards an Understanding of Synapse Formation. Neuron *100*, 276–293. https://doi.org/10.1016/j.neuron.2018.09.040.

2. Schreiner, D., Savas, J.N., Herzog, E., Brose, N., and de Wit, J. (2017). Synapse biology in the 'circuit-age'-paths toward molecular connectomics. Curr. Opin. Neurobiol. *42*, 102–110. https://doi.org/10.1016/j.conb.2016.12.004.

3. Chowdhury, D., Watters, K., and Biederer, T. (2021). Synaptic recognition molecules in development and disease. Curr. Top. Dev. Biol. *142*, 319–370. https://doi.org/10.1016/bs.ctdb.2020.12.009.

4. Südhof, T.C. (2017). Synaptic Neurexin Complexes: A Molecular Code for the Logic of Neural Circuits. Cell *171*, 745–769. https://doi.org/10.1016/j.cell.2017.10.024.

5. Reissner, C., Runkel, F., and Missler, M. (2013). Genome Biol. *14*, 213. https://doi.org/10.1186/gb-2013-14-9-213.

6. Gomez, A.M., Traunmüller, L., and Scheiffele, P. (2021). Neurexins: molecular codes for shaping neuronal synapses. Nat. Rev. Neurosci. *22*, 137–151. https://doi.org/10.1038/s41583-020-00415-7.

7. Glessner, J.T., Wang, K., Cai, G., Korvatska, O., Kim, C.E., Wood, S., Zhang, H., Estes, A., Brune, C.W., Bradfield, J.P., et al. (2009). Autism genome-wide copy number variation reveals ubiquitin and neuronal genes. Nature *459*, 569–573. https://doi.org/10.1038/nature07953.

8. De Rubeis, S., He, X., Goldberg, A.P., Poultney, C.S., Samocha, K., Cicek, A.E., Kou, Y., Liu, L., Fromer, M., Walker, S., et al. (2014). Synaptic, transcriptional and chromatin genes disrupted in autism. Nature *515*, 209–215. https://doi.org/10.1038/nature13772.

9. Castronovo, P., Baccarin, M., Ricciardello, A., Picinelli, C., Tomaiuolo, P., Cucinotta, F., Frittoli, M., Lintas, C., Sacco, R., and Persico, A.M. (2020). Phenotypic spectrum of NRXN1 mono- and bi-allelic deficiency: A systematic review. Clin. Genet. *97*, 125–137. https://doi.org/10.1111/cge.13537.

10. Marshall, C.R., Howrigan, D.P., Merico, D., Thiruvahindrapuram, B., Wu, W., Greer, D.S., Antaki, D., Shetty, A., Holmans, P.A., Pinto, D., et al. (2017). Contribution of copy number variants to schizophrenia from a genome-wide study of 41,321 subjects. Nat. Genet. *49*, 27–35. https://doi.org/10.1038/ng.3725.

11. Huang, A.Y., Yu, D., Davis, L.K., Sul, J.H., Tsetsos, F., Ramensky, V., Zelaya, I., Ramos, E.M., Osiecki, L., Chen, J.A., et al. (2017). Rare Copy Number Variants in NRXN1 and CNTN6 Increase Risk for Tourette Syndrome. Neuron *94*, 1101–1111.e7. https://doi.org/10.1016/j.neuron.2017.06.010.

12. Schreiner, D., Nguyen, T.M., Russo, G., Heber, S., Patrignani, A., Ahrné, E., and Scheiffele, P. (2014). Targeted combinatorial alternative splicing generates brain region-specific repertoires of neurexins. Neuron *84*, 386–398. https://doi.org/10.1016/j.neuron.2014.09.011 S0896-6273(14)00799-5.

13. Treutlein, B., Gokce, O., Quake, S.R., and Südhof, T.C. (2014). Cartography of neurexin alternative splicing mapped by single-molecule long-read mRNA sequencing. Proc. Natl. Acad. Sci. USA *111*, E1291–E1299. https://doi.org/10.1073/pnas.1403244111.

14. Ray, T.A., Cochran, K., Kozlowski, C., Wang, J., Alexander, G., Cady, M.A., Spencer, W.J., Ruzycki, P.A., Clark, B.S., Laeremans, A., et al. (2020). Comprehensive identification of mRNA isoforms reveals the diversity of neural cell-surface molecules with roles in retinal development and disease. Nat. Commun. *11*, 3328. https://doi.org/10.1038/s41467-020-17009-7.

15. Zhang, P., Lu, H., Peixoto, R.T., Pines, M.K., Ge, Y., Oku, S., Siddiqui, T.J., Xie, Y., Wu, W., Archer-Hartmann, S., et al. (2018). Heparan Sulfate Organizes Neuronal Synapses Through Neurexin Partnerships. Cell *174*, 1450–1464.e23. https://doi.org/10.1016/j.cell.2018.07.002.

16. Xu, D., and Esko, J.D. (2014). Demystifying heparan sulfate-protein interactions. Annu. Rev. Biochem. *83*, 129–157. https://doi.org/10.1146/annurev-biochem-060713-035314.

17. Reily, C., Stewart, T.J., Renfrow, M.B., and Novak, J. (2019). Glycosylation in health and disease. Nat. Rev. Nephrol. *15*, 346–366. https://doi.org/10.1038/s41581-019-0129-4.

18. Langford, J.K., Stanley, M.J., Cao, D., and Sanderson, R.D. (1998). Multiple heparan sulfate chains are required for optimal syndecan-1 function. J. Biol. Chem. *273*, 29965–29971.

19. Gopal, S., Bober, A., Whiteford, J.R., Multhaupt, H.A.B., Yoneda, A., and Couchman, J.R. (2010). Heparan sulfate chain valency controls syndecan-4 function in cell adhesion. J. Biol. Chem. *285*, 14247–14258. https://doi.org/10.1074/jbc.M109.056945.

20. Yuzaki, M. (2018). Two Classes of Secreted Synaptic Organizers in the Central Nervous System. Annu. Rev. Physiol. *80*, 243–262. https://doi.org/10.1146/annurev-physiol-021317-121322.

21. Etherton, M.R., Blaiss, C.A., Powell, C.M., and Südhof, T.C. (2009). Mouse neurexin-1alpha deletion causes correlated electrophysiological and behavioral changes consistent with cognitive impairments. Proc. Natl. Acad. Sci. USA *106*, 17998–18003.

22. Pak, C., Danko, T., Zhang, Y., Aoto, J., Anderson, G., Maxeiner, S., Yi, F., Wernig, M., and Südhof, T.C. (2015). Human Neuropsychiatric Disease Modeling using Conditional Deletion Reveals Synaptic Transmission Defects Caused by Heterozygous Mutations in NRXN1. Cell Stem Cell *17*, 316–328. https://doi.org/10.1016/j.stem.2015.07.017.

23. Armstrong, E.C., Caruso, A., Servadio, M., Andreae, L.C., Trezza, V., Scattoni, M.L., and Fernandes, C. (2020). Assessing the developmental trajectory of mouse models of neurodevelopmental disorders: Social and communication deficits in mice with Neurexin 1alpha deletion. Gene Brain Behav. *19*, e12630. https://doi.org/10.1111/gbb.12630.

24. Grayton, H.M., Missler, M., Collier, D.A., and Fernandes, C. (2013). Altered social behaviours in neurexin 1alpha knockout mice resemble core symptoms in neurodevelopmental disorders. PLoS One *8*, e67114. https://doi.org/10.1371/journal.pone.0067114 PONE-D-13-12674.

25. Xu, B., Ho, Y., Fasolino, M., Medina, J., O'Brien, W.T., Lamonica, J.M., Nugent, E., Brodkin, E.S., Fuccillo, M.V., Bucan, M., and Zhou, Z. (2023). Allelic contribution of Nrxn1alpha to autism-relevant behavioral phenotypes in mice. PLoS Genet. *19*, e1010659. https://doi.org/10.1371/journal.pgen.1010659.

26. Dai, J., Aoto, J., and Südhof, T.C. (2019). Alternative Splicing of Presynaptic Neurexins Differentially Controls Postsynaptic NMDA and AMPA Receptor Responses. Neuron *102*, 993–1008.e5. https://doi.org/10.1016/j.neuron.2019.03.032.

27. Traunmüller, L., Gomez, A.M., Nguyen, T.M., and Scheiffele, P. (2016). Control of neuronal synapse specification by a highly dedicated alternative splicing program. Science *352*, 982–986. https://doi.org/10.1126/science.aaf2397.

28. Furlanis, E., Traunmüller, L., Fucile, G., and Scheiffele, P. (2019). Landscape of ribosome-engaged transcript isoforms reveals extensive neuronal-cell-class-specific alternative splicing programs. Nat. Neurosci. *22*, 1709–1717. https://doi.org/10.1038/s41593-019-0465-5.

29. Flaherty, E., Zhu, S., Barretto, N., Cheng, E., Deans, P.J.M., Fernando, M.B., Schrode, N., Francoeur, N., Antoine, A., Alganem, K., et al. (2019). Neuronal impact of patient-specific aberrant NRXN1alpha splicing. Nat. Genet. *51*, 1679–1690. https://doi.org/10.1038/s41588-019-0539-z.

30. Trotter, J.H., Dargaei, Z., Sclip, A., Essayan-Perez, S., Liakath-Ali, K., Raju, K., Nabet, A., Liu, X., Wohr, M., and Sudhof, T.C. (2021). Compartment-Specific Neurexin Nanodomains Orchestrate Tripartite Synapse Assembly. Preprint at bioRxiv. https://doi.org/10.1101/2020.08.21.262097.

31. Lukacsovich, D., Winterer, J., Que, L., Luo, W., Lukacsovich, T., and Földy, C. (2019). Single-Cell RNA-Seq Reveals Developmental Origins and Ontogenetic Stability of Neurexin Alternative Splicing Profiles. Cell Rep. *27*, 3752–3759.e4. https://doi.org/10.1016/j.celrep.2019.05.090.

32. Missler, M., Zhang, W., Rohlmann, A., Kattenstroth, G., Hammer, R.E., Gottmann, K., and Südhof, T.C. (2003). Alpha-neurexins couple Ca2+ channels to synaptic vesicle exocytosis. Nature *423*, 939–948. https://doi.org/10.1038/nature01755.

33. Anderson, G.R., Aoto, J., Tabuchi, K., Földy, C., Covy, J., Yee, A.X., Wu, D., Lee, S.J., Chen, L., Malenka, R.C., and Südhof, T.C. (2015). beta-Neurexins Control Neural Circuits by Regulating Synaptic Endocannabinoid Signaling. Cell *162*, 593–606. https://doi.org/10.1016/j.cell.2015.06.056.

34. David, G., Bai, X.M., Van der Schueren, B., Cassiman, J.J., and Van den Berghe, H. (1992). Developmental changes in heparan sulfate expression: in situ detection with mAbs. J. Cell Biol. *119*, 961–975.

35. Esko, J.D., and Zhang, L. (1996). Influence of core protein sequence on glycosaminoglycan assembly. Curr. Opin. Struct. Biol. *6*, 663–670. https://doi.org/10.1016/s0959-440x(96)80034-0.

36. Oku, S., Feng, H., Connor, S., Toledo, A., Zhang, P., Zhang, Y., Thoumine, O., Zhang, C., and Craig, A.M. (2020). Alternative splicing at neuroligin site A regulates glycan interaction and synaptogenic activity. Elife *9*, e58668. https://doi.org/10.7554/eLife.58668.

37. Dean, C., Scholl, F.G., Choih, J., DeMaria, S., Berger, J., Isacoff, E., and Scheiffele, P. (2003). Neurexin mediates the assembly of presynaptic terminals. Nat. Neurosci. *6*, 708–716.

38. Kim, J.H., Lee, S.R., Li, L.H., Park, H.J., Park, J.H., Lee, K.Y., Kim, M.K., Shin, B.A., and Choi, S.Y. (2011). High cleavage efficiency of a 2A peptide derived from porcine teschovirus-1 in human cell lines, zebrafish and mice. PLoS One *6*, e18556. https://doi.org/10.1371/journal.pone.0018556.

39. Fuccillo, M.V., Földy, C., Gökce, Ö., Rothwell, P.E., Sun, G.L., Malenka, R.C., and Südhof, T.C. (2015). Single-Cell mRNA Profiling Reveals Cell-Type-Specific Expression of Neurexin Isoforms. Neuron *87*, 326–340. https://doi.org/10.1016/j.neuron.2015.06.028.

40. Harris, K.M., and Kater, S.B. (1994). Dendritic spines: cellular specializations imparting both stability and flexibility to synaptic function. Annu. Rev. Neurosci. *17*, 341–371.

41. Kaeser, P.S., and Regehr, W.G. (2017). The readily releasable pool of synaptic vesicles. Curr. Opin. Neurobiol. *43*, 63–70. https://doi.org/10.1016/j.conb.2016.12.012.

42. Budreck, E.C., Kwon, O.B., Jung, J.H., Baudouin, S., Thommen, A., Kim, H.S., Fukazawa, Y., Harada, H., Tabuchi, K., Shigemoto, R., et al. (2013). Neuroligin-1 controls synaptic abundance of NMDA-type glutamate receptors through extracellular coupling. Proc. Natl. Acad. Sci. USA *110*, 725–730. https://doi.org/10.1073/pnas.1214718110.

43. Bhouri, M., Morishita, W., Temkin, P., Goswami, D., Kawabe, H., Brose, N., Südhof, T.C., Craig, A.M., Siddiqui, T.J., and Malenka, R. (2018). Deletion of LRRTM1 and LRRTM2 in adult mice impairs basal AMPA receptor transmission and LTP in hippocampal CA1 pyramidal neurons. Proc. Natl. Acad. Sci. USA *115*, E5382–E5389. https://doi.org/10.1073/pnas.1803280115.

44. Ramsey, A.M., Tang, A.H., LeGates, T.A., Gou, X.Z., Carbone, B.E., Thompson, S.M., Biederer, T., and Blanpied, T.A. (2021). Subsynaptic positioning of AMPARs by LRRTM2 controls synaptic strength. Sci. Adv. *7*, eabf3126. https://doi.org/10.1126/sciadv.abf3126.

45. Matsuda, K., Budisantoso, T., Mitakidis, N., Sugaya, Y., Miura, E., Kakegawa, W., Yamasaki, M., Konno, K., Uchigashima, M., Abe, M., et al. (2016). Transsynaptic Modulation of Kainate Receptor Functions by C1q-like Proteins. Neuron *90*, 752–767. https://doi.org/10.1016/j.neuron.2016.04.001.

46. Hauser, D., Behr, K., Konno, K., Schreiner, D., Schmidt, A., Watanabe, M., Bischofberger, J., and Scheiffele, P. (2022). Targeted proteoform mapping uncovers specific Neurexin-3 variants required for dendritic inhibition. Neuron *110*, 2094–2109.e10. https://doi.org/10.1016/j.neuron.2022.04.017.

47. Montoliu-Gaya, L., Tietze, D., Kaminski, D., Mirgorodskaya, E., Tietze, A.A., and Sterky, F.H. (2021). CA10 regulates neurexin heparan sulfate addition via a direct binding in the secretory pathway. EMBO Rep. *22*, e51349. https://doi.org/10.15252/embr.202051349.

48. Khalaj, A.J., Sterky, F.H., Sclip, A., Schwenk, J., Brunger, A.T., Fakler, B., and Südhof, T.C. (2020). Deorphanizing FAM19A proteins as pan-neurexin ligands with an unusual biosynthetic binding mechanism. J. Cell Biol. *219*, e202004164. https://doi.org/10.1083/jcb.202004164.

49. Luo, F., Sclip, A., Jiang, M., and Südhof, T.C. (2020). Neurexins cluster Ca(2+) channels within the presynaptic active zone. EMBO J. *39*, e103208. https://doi.org/10.15252/embj.2019103208.

50. Brockhaus, J., Schreitmüller, M., Repetto, D., Klatt, O., Reissner, C., Elmslie, K., Heine, M., and Missler, M. (2018). alpha-Neurexins Together with alpha2delta-1 Auxiliary Subunits Regulate Ca(2+) Influx through Cav2.1 Channels. J. Neurosci. *38*, 8277–8294. https://doi.org/10.1523/JNEUROSCI.0511-18.2018.

51. Ju, A., Hammerschmidt, K., Tantra, M., Krueger, D., Brose, N., and Ehrenreich, H. (2014). Juvenile manifestation of ultrasound communication deficits in the neuroligin-4 null mutant mouse model of autism. Behav. Brain Res. *270*, 159–164. https://doi.org/10.1016/j.bbr.2014.05.019 S0166-4328(14)00313-1.

52. Wöhr, M. (2014). Ultrasonic vocalizations in Shank mouse models for autism spectrum disorders: detailed spectrographic analyses and developmental profiles. Neurosci. Biobehav. Rev. *43*, 199–212. https://doi.org/10.1016/j.neubiorev.2014.03.021.

53. Pettem, K.L., Yokomaku, D., Takahashi, H., Ge, Y., and Craig, A.M. (2013). Interaction between autism-linked MDGAs and neuroligins suppresses inhibitory synapse development. J. Cell Biol. *200*, 321–336. https://doi.org/10.1083/jcb.201206028.

54. Coffey, K.R., Marx, R.E., and Neumaier, J.F. (2019). DeepSqueak: a deep learning-based system for detection and analysis of ultrasonic vocalizations. Neuropsychopharmacology *44*, 859–868. https://doi.org/10.1038/s41386-018-0303-6.

55. Friard, O., and Gamba, M. (2016). BORIS: a free, versatile open-source event-logging software for video/audio coding and live observations. Methods Ecol. Evol. *7*, 1325–1330. https://doi.org/10.1111/2041-210X.12584.

56. Kaech, S., and Banker, G. (2006). Culturing hippocampal neurons. Nat. Protoc. *1*, 2406–2415. https://doi.org/10.1038/nprot.2006.356.

57. Takahashi, H., Arstikaitis, P., Prasad, T., Bartlett, T.E., Wang, Y.T., Murphy, T.H., and Craig, A.M. (2011). Postsynaptic TrkC and presynaptic PTPsigma function as a bidirectional excitatory synaptic organizing complex. Neuron *69*, 287–303. https://doi.org/10.1016/j.neuron.2010.12.024.

58. Bischofberger, J., Engel, D., Li, L., Geiger, J.R.P., and Jonas, P. (2006). Patch-clamp recording from mossy fiber terminals in hippocampal slices. Nat. Protoc. *1*, 2075–2081. https://doi.org/10.1038/nprot.2006.312.

59. Blaney, C.E., Gunn, R.K., Stover, K.R., and Brown, R.E. (2013). Maternal genotype influences behavioral development of 3xTg-AD mouse pups. Behav. Brain Res. *252*, 40–48. https://doi.org/10.1016/j.bbr.2013.05.033 S0166-4328(13)00312-4.

60. Dierssen, M., Fotaki, V., Martínez de Lagrán, M., Gratacós, M., Arbonés, M., Fillat, C., and Estivill, X. (2002). Neurobehavioral development of two mouse lines commonly used in transgenic studies. Pharmacol. Biochem. Behav. *73*, 19–25. https://doi.org/10.1016/s0091-3057(02)00792-x.

61. Fox, W.M. (1965). Reflex-ontogeny and behavioural development of the mouse. Anim. Behav. *13*, 234–241. https://doi.org/10.1016/0003-3472(65)90041-2.

62. Tremml, P., Lipp, H.P., Müller, U., Ricceri, L., and Wolfer, D.P. (1998). Neurobehavioral development, adult openfield exploration and swimming navigation learning in mice with a modified beta-amyloid precursor protein gene. Behav. Brain Res. *95*, 65–76. https://doi.org/10.1016/s0166-4328(97)00211-8.

63. Hill, J.M., Lim, M.A., and Stone, M.M. (2008). Developmental Milestones in the Newborn Mouse. In Neuropeptide Techniques I. Gozes (Humana Press), pp. 131–149. https://doi.org/10.1007/978-1-60327-099-1_10.

64. Branchi, I., Santucci, D., and Alleva, E. (2001). Ultrasonic vocalisation emitted by infant rodents: a tool for assessment of neurobehavioural development. Behav. Brain Res. *125*, 49–56. https://doi.org/10.1016/s0166-4328(01)00277-7.

65. Kalueff, A.V., Aldridge, J.W., LaPorte, J.L., Murphy, D.L., and Tuohimaa, P. (2007). Analyzing grooming microstructure in neurobehavioral experiments. Nat. Protoc. *2*, 2538–2544. https://doi.org/10.1038/nprot.2007.367.

STAR★METHODS

KEY RESOURCES TABLE

REAGENT or RESOURCE	SOURCE	IDENTIFIER
Antibodies		
Mouse anti-HS stub (3G10)	AMSBIO LLC	Cat# 370260-1; RRID: AB_10892311
Mouse anti-V5	ThermoFisher	Cat# R960-25; RRID: AB_2556564
Rabbit anti-V5	Cell Signaling Technology	Cat# 13202; RRID: AB_2687461
Rabbit anti-Nrxn1	Synaptic Systems	Cat# 175103 RRID: AB_10697816
Rabbit anti-pan-Nrxn	Millipore	Cat#ABN161; RRID: AB_10917110
Mouse anti-alpha-tubulin	Millipore	Cat# 05–829; RRID: AB_310035
Chicken anti-MAP2	Abcam	Cat# ab5392; RRID: AB_2138153
Rabbit anti-Myc	Sigma	Cat#C3956; RRID: AB_439680
Mouse anti-Bassoon	Enzo Life Sciences	Cat# ADI-VAM-PS003-F; RRID: AB_11181058
Mouse anti-PSD-95	ThermoFisher	Cat# MA1-045; RRID: AB_325399
Mouse anti-PSD-95	ThermoFisher	Cat# MA1-046; RRID: AB_2092361
Guinea pig anti-VGAT	Synaptic Systems	Cat# 131 004; RRID: AB_887873
Mouse anti-Gephyrin	Synaptic Systems	Cat# 147 021; RRID: AB_2232546
Mouse anti-VGluT1	NeuroMab	Cat# 75-066; RRID: AB_2877383
Mouse anti-ELKS	Sigma	Cat# E4531; RRID: AB_2100013
Bacterial and virus strains		
AAV6-GFP-4xshRNA	(Zhang et al.)[15]	N/A
AAV6-rNrxn-TKD	(Zhang et al.)[15]	N/A
Chemicals, peptides, and recombinant proteins		
Nrxn1α(SA)-AP-Myc-His	This paper	N/A
Nrxn1α(ΔGAG)-AP-Myc-His	This paper	N/A
NL1-Fc	This paper	N/A
NL2-Fc	This paper	N/A
LRRTM2-Fc	This paper	N/A
Tetrodotoxin (TTX)	Abcam	Cat# ab120054
Bicuculline methiodide	Abcam	Cat# ab120109
DL-APV	Abcam	Cat# ab120271
Critical commercial assays		
Heparinase I	Sigma	Cat# H2519
Heparinase II	Sigma	Cat# H6512
Heparinase III	Sigma	Cat# H8891
Experimental models: Cell lines		
Human: HEK293 cells	ATCC	Cat# CRL-1573
Rat: embryonic day 18 hippocampal primary neuron culture	This paper	N/A
Experimental models: Organisms/strains		
Mouse: C57BL/6J	The Jackson Laboratory	JAX: 000664; RRID: IMSR_JAX:000664
Mouse: *Nrxn1*$^{\Delta S5}$	This paper	N/A
Oligonucleotides		
Nrxn1 ratiometric RT-PCR forward primer: 5′-AGGACATTGACCCCTGTGAG-3′	This paper	N/A

(*Continued on next page*)

Continued

REAGENT or RESOURCE	SOURCE	IDENTIFIER
Nrxn1 ratiometric RT-PCR reverse primer: 5′-CACCTACTCTGGTGGGGTTG-3′	This paper	N/A
PCR primers used for qPCR: See Table S2	This paper	N/A
Recombinant DNA		
pLL3.7-hSyn-CFP-P2A-V5-Nrxn1α(-S5)	(Zhang et al.)[15]	N/A
pLL3.7-hSyn-CFP-P2A-V5-Nrxn1α(+S5)	This paper	N/A
pLL3.7-hSyn-YFP-P2A-V5-Nrxn1β(-S5)	(Zhang et al.)[15]	N/A
pLL3.7-hSyn-YFP-P2A-V5-Nrxn1β(+S5)	This paper	N/A
pLL3.7-hSyn-YFP-P2A-V5-Nrxn1β(+S5)AAGGL	This paper	N/A
pLL3.7-hSyn-V5-Nrxn1β(-S5)	(Zhang et al.)[15]	N/A
pLL3.7-hSyn-V5-Nrxn1β(-S5)SA	(Zhang et al.)[15]	N/A
pLL3.7-hSyn-V5-Nrxn1β(+S5)	This paper	N/A
pLL3.7-hSyn-V5-Nrxn1β(+S5)SA	This paper	N/A
pLL3.7-hSyn-V5-Nrxn1β(+S5)ΔGAG	This paper	N/A
pcDNA4-Nrxn1α(SA)-PLAP-Myc-His	This paper	N/A
pcDNA4-Nrxn1α(ΔGAG)-PLAP-Myc-His	(Zhang et al.)[15]	N/A
pcDNA4-NL1-Fc	(Pettem et al.)[53]	N/A
pcDNA4-NL2-Fc	(Pettem et al.)[53]	N/A
pcDNA4-LRRTM2-Fc	This paper	N/A
pLL3.7-hSyn-YFP-MDGA1	(Pettem et al.)[53]	N/A
pLL3.7-hSyn-V5-Nrxn1β(-S5)-SEP	This paper	N/A
pLL3.7-hSyn-V5-Nrxn1β(+S5)-SEP	This paper	N/A
Software and algorithms		
pCLAMP 10	Molecular Devices	
Mini Analysis	Synaptosoft	http://www.synaptosoft.com/MiniAnalysis/
GraphPad Prism 8	GraphPad Software Inc.	https://www.graphpad.com/scientific-software/prism/
R	R Foundation for Statistical Computing	www.R-project.org
DeepSqueak	(Coffey et al.)[54]	https://github.com/DrCoffey/DeepSqueak
BORIS	(Friard et al.)[55]	http://www.boris.unito.it.
Image Lab	Bio-Rad	http://www.bio-rad.com/en-ca/product/image-lab-software
ImageJ	National Institute of Health	https://ImageJ.nih.gov/ij/index.html
Quantity One	Bio-Rad	https://www.bio-rad.com/fr-ca/product/quantity-one-1-d-analysis-software
Zen Blue	Zeiss	https://www.zeiss.com/microscopy/int/products/microscope-software/zen.html
RECONSTRUCT	SynapseWeb	https://synapseweb.clm.utexas.edu/software-0

RESOURCE AVAILABILITY

Lead contact

Further information and requests for resources and reagents should be directed to and will be fulfilled by the lead contact, Ann Marie Craig (acraig@mail.ubc.ca).

Materials availability

All unique renewable materials and reagents will be available upon reasonable request to the lead contact. A completed Materials Transfer Agreement may be required.

Data and code availability

- All data generated in this study will be made available upon reasonable request.

- This paper does not report original code.
- Any additional information regarding the data reported in this work is available from the lead contact upon request.

EXPERIMENTAL MODEL AND STUDY PARTICIPANT DETAILS

Mice

The *Nrxn1*$^{\Delta S5}$ knock-in mouse line was custom generated by The Jackson Laboratory on a C57BL/6J background. Three bp substitution mutations were introduced in embryos through injection of Cas9 mRNA, a guide RNA against Nrxn1 exon 22, and donor ssDNA oligonucleotide with targeted mutations (described in Figure S2A). Mouse genotyping was performed by PCR and sequencing, and the targeted mutations confirmed by sequencing after germline transmission. Primers used for routine genotyping are Nrxn1_genoF1: ATCACCACTTCTGTGTCCAC and Nrxn1_genoR: GAAATCCTTATCCTCTGTCC. The size of the PCR products are 551 bp from both wild-type and *Nrxn1*$^{\Delta S5}$ knock-in mice. They are then sent for direct Sanger sequencing to check for the three-bp mutation using sequencing primer Nrxn1_genoF: AGTTCAGTGTCTTGAGGAAG. The wild-type mice generated from initial heterozygous *Nrxn1*$^{\Delta S5/+}$ crosses were bred in parallel to generate age-matched controls for all experiments. Mice were limited to 10 generations of inbreeding before backcrossing with C57BL/6J mice from The Jackson Laboratory to mitigate genetic drift. Mice were housed in breeding pairs or in same-sex groups of 2–5 with free access to food and water under specific pathogen-free conditions. Survival rates were not significantly different between males and females and data were pooled. Mice were procedure- and test-naive for all experiments except where indicated below. Mice for biochemistry and electrophysiology were housed in a regular 12-h light/dark cycle. All procedures were approved by the Animal Care Committees at the University of British Columbia and at Dalhousie University.

Primary neuron culture

Primary rat hippocampal or cortical neuron cultures were prepared from embryonic day 18 pooled male and female rat embryos.[56] Briefly, hippocampal neurons were cultured at low density on poly-L-lysine-coated glass coverslips inverted over a feeder layer of astroglial cells in neurobasal medium (Invitrogen) supplemented with B27. Cytosine arabinoside (5 μM) was added to hippocampal neuron culture dishes at 2 days *in vitro* (DIV) to prevent overgrowth of glial cells. Cortical neurons were cultured on poly-L-lysine-coated 12-well plates in the same medium. WT and *Nrxn1*$^{\Delta S5/\Delta S5}$ mouse hippocampal neuron cultures were generated from *Nrxn1*$^{-\Delta S5/+}$ x *Nrxn1*$^{\Delta S5/+}$ crosses, derived from timed-pregnant dams at embryonic days 17–18. Mouse hippocampi were dissected from individual embryos and stored at 4°C in Hibernate E (Invitrogen) pending parallel genotyping of tail tissue. Mouse neurons were dissociated using papain (20 units/ml, 15 min, 37°C) and cultured as described above for rat hippocampal neurons with additional 25 μg/mL bovine pancreatic insulin (Sigma) in the media.

Cell line culture

Human embryonic kidney 293 (HEK293) cells were cultured in Dulbecco's Modified Eagle's medium (DMEM; Invitrogen) supplemented with 10% bovine growth serum (BGS). This line was obtained from ATCC and is not authenticated.

METHOD DETAILS

Plasmid constructs

All Nrxn1 constructs use mouse cDNAs lacking the S4 insert to allow binding to LRRTMs. For expression in neurons, pLL3.7-hSyn-CFP-P2A-V5-Nrxn1α(-S5), pLL3.7-hSyn-V5-Nrxn1β(-S5), and pLL3.7-hSyn-YFP-P2A-V5-Nrxn1β(-S5)[15] were modified by site-directed mutagenesis to generate pLL3.7-hSyn-CFP-P2A-V5-Nrxn1α(+S5), pLL3.7-hSyn-V5-Nrxn1β(+S5), and pLL3.7-hSyn-YFP-P2A-V5-Nrxn1β(+S5), respectively. Producing the +S5 isoform required the addition of the short 3-amino acid S5 insert, GGL. Nrxn1 α and β rescue constructs were mutated to be shRNA resistant while leaving original protein sequences intact. pLL3.7-hSyn-V5-Nrxn1β(+S5)SA was generated by site-directed mutagenesis from pLL3.7-hSyn-V5-Nrxn1β(-S5)SA.[15] The SA mutants have a single amino acid mutation at the constitutive HS site of Nrxn1, converting the serine residue to alanine, SA (316). pLL3.7-hSyn-V5-Nrxn1β(+S5)ΔGAG was generated based on pLL3.7-hSyn-V5-Nrxn1β(+S5)SA by further introducing two additional serine to alanine mutations at the serines adjacent to S5, SSAA (332, 333). pLL3.7-hSyn-YFP-P2A-V5-Nrxn1β(+S5) AAGGL was generated by mutating these two serines adjacent to S5 to alanines in pLL3.7-hSyn-YFP-P2A-V5-Nrxn1β(+S5). pLL3.7-hSyn-V5-Nrxn1β(-S5)-SEP was derived from pLL3.7-hSyn-V5-Nrxn1β(-S5), inserting the SEP sequence immediately before exon 20 (corresponds to splice site 4 in Nrxn1 isoforms with the S4 insert). Site-directed mutagenesis was used to modify pLL3.7-hSyn-V5-Nrxn1β(-S5)-SEP to generate pLL3.7-hSyn-V5-Nrxn1β(+S5)-SEP. pLL3.7-hSyn-YFP-MDGA1[53] expresses YFP-tagged surface protein MDGA1 which can be clustered by the anti-GFP-coated beads as a negative control for presynaptic differentiation. Nrxn1 constructs used for protein purification were based on pcDNA4-Nrxn1α(ΔGAG)-PLAP-Myc-His.[15] pcDNA4-Nrxn1α(SA)-PLAP-Myc-His was generated by switching the two alanines adjacent to S5 back to serine by site-directed mutagenesis, leaving just the constitutive HS site mutated. pcDNA4-NL1-Fc and pcDNA4-NL2-Fc[53] express neuroligin ectodomains fused to Fc. pcDNA4-LRRTM2-Fc was made by subcloning the mature extracellular region of LRRTM2 (aa 34–421) between the neurexin1β signal sequence and the human IgG Fc cDNA in the vector pc4-sp-Fc modified from pcDNA4.[57]

Neurexin molecular replacement in culture

For Nrxn triple knockdown and rescue experiments, hippocampal neurons were transfected at DIV 0 using AMAXA nucleofection (Lonza). Constructs used were shRNA-resistant CFP-P2A-V5-Nrxn1α and V5-Nrxn1β with or without the S5 insert mixed at a 10:1 ratio of α:β plasmid, or the same amount of CFP vector only, all using the same pLL3.7-hSyn vector backbone. For AAV-mediated Nrxn knockdown, Nrxn triple knockdown AAV vector AAV6-rNrx-TKD (shNrxn) or control AAV6-GFP-4xshRNA (shCon) was used.[15] One round of AAV infection was done on DIV 3 and repeated at DIV 6.

Whole-cell patch clamp recordings of mEPSCs were performed in cultured hippocampal neurons at room temperature at DIV 14. Neurons were continuously perfused (1 mL/min) with the extracellular solution containing (in mM): NaCl 140, $CaCl_2$ 1.3, KCl 5.4, $MgCl_2$ 1, HEPES 25, glucose 33 (pH 7.35). Tetrodotoxin (0.5 μM; Abcam), bicuculline methiodide (10 μM; Abcam), and DL-2-Amino-5-phosphonopentanoic acid sodium salt (APV, 100 μM; Abcam) were added prior to recordings to block action potentials, GABA receptor-mediated inhibitory synaptic currents, and NMDA receptor-mediated excitatory synaptic currents, respectively. Patch pipettes were pulled from borosilicate glass capillary tubes (World Precision Instruments) using a PP-830 pipette puller (Narishige). The resistance of pipettes varied between 4 and 6 MΩ. The patch pipette solution contained (in mM): Cs gluconate 122.5, CsCl 17.5, $MgCl_2$ 2, HEPES 10, BAPTA 10, ATP 4, and QX314 5 (pH 7.2). Neurons were voltage clamped at −60 mV, and recorded with a MultiClamp 700B amplifier (Molecular Devices). Records were filtered at 2 kHz, and acquired with pCLAMP 10 software (Molecular Devices). The series resistance in the recordings varied between 6 and 10 MΩ, and recordings where series resistance varied by more than 10% were rejected. Electronic compensation for series resistance was not employed, and cells that demonstrated a change in "leak" current of more than 10% were rejected from the analysis. Traces were analyzed using the MiniAnalysis 6.0 software (Synaptosoft). Analyses were done by experimenters blind to the experimental groups.

Neuron culture immunoprecipitation

Cortical neurons were transfected at DIV 0 using AMAXA nucleofection (Lonza) with the series of pLL3.7-hSyn-V5-Nrxn1β constructs. At DIV 18–19, cultured cortical neurons were washed with chilled PBS twice and lysed in cold lysis buffer (50 mM Tris-HCl pH 7.4, 150 mM NaCl, 1% Triton X-100, 0.03% deoxycholic acid sodium, supplemented with Protease Inhibitor Cocktail (Roche)). Lysate was centrifuged for 20 min at 21,130 g at 4°C, after which supernatant was incubated with anti-V5 (Millipore, AB3792) antibody for 2 h at 4°C. Protein G agarose was added to the lysates and samples were rotated overnight at 4°C. After three washes with wash buffer (20 mM M Tris-HCl, pH 7.4, 150 mM NaCl, 0.1% Triton X-100, protease inhibitors), samples were treated with or without Heparinase I, II, and III (1 U/ml) for 2 h at 37°C. The resulting samples were dissolved in SDS loading buffer and run on 10% polyacrylamide gels. Gels were transferred onto Immobilon P membranes which were blocked in 5% skim milk and 3% BSA in Tris-buffered saline/0.05% Tween 20 for an hour at room temperature followed with 3G10 anti-heparan sulfate stub region (1:3000; AMSBIO). Membranes were then incubated with goat anti-mouse HRP conjugated secondary antibody (SouthernBiotech 1030-05) for chemiluminescence. The Immobilon Western Chemiluminescent HRP Substrate (Millipore WBKLS0500) was used for signal detection. Immunoblots were then stripped at 55°C for 15 min, washed three times with Tris-buffered saline/0.025% Tween 20, blocked with 5% milk, and probed with anti-V5 (1:5000; Thermo Fisher Scientific, R960-CUS).

Ectodomain fusion protein production

For purification of recombinant Nrxn1α proteins, pcDNA4-Nrxn1α+S5-PLAP-Myc-His or pcDNA4-Nrxn1αΔGAG-PLAP-Myc-His was transfected with TransIT-LT1 (Mirus Bio) into HEK293 cells cultured in DMEM with 10% BGS for four weeks in the presence of 0.5 mg/mL Zeocin. Zeocin-selected cells were grown in serum-free AIM V media for an additional four weeks, during which media was collected every three days. For purification of recombinant proteins used for ligand binding assays, either stable cell lines were generated and conditioned media collected as above or constructs were transiently transfected into HEK293 cells. For transient transfection, polyethylenimine branched (Sigma 408727) was used, cells were switched to serum-free DMEM 24 h post-transfection and media collected over the next 48 h. Conditioned media was concentrated in PBS with Centricon Plus-70 filters (Millipore). Recombinant His-tagged proteins were purified using Ni-NTA agarose beads (QIAGEN) and eluted with 200 mM imidazole. Recombinant Fc-tagged proteins were purified using Protein G beads (GE Healthcare) and eluted with 0.2 M glycine (pH 2.5) followed by addition of 1 M Tris-HCl (pH 8.5) to neutralize pH. Purified proteins were then washed with PBS and concentrated using Amicon Ultra-15 centrifugal filter units (50 kDa cutoff, Millipore). Protein concentrations were quantitated by SDS-PAGE with bovine serum albumin standards using Sypro Ruby gel stain.

Immunocytochemistry

All imaging and analyses were done blind to experimental conditions. Coverslips with hippocampal neurons were fixed for 12 min using warm parafix (4% paraformaldehyde and 4% sucrose in PBS, pH 7.4). Fixation was followed by permeabilization with 0.2% Triton X-100 in PBS, except for experiments that required surface staining. Coverslips were blocked with blocking solution (3% bovine serum albumin and 5% normal goat serum in PBS) for 30 min at 37°C and then incubated with primary antibodies in the blocking solution overnight at 4°C. Neurons were then incubated with the appropriate Alexa Fluor-conjugated (1:1000, Invitrogen; Alexa 488, Alexa 568, and Alexa 647) or AMCA-conjugated (donkey IgG; 1:400; Jackson ImmunoResearch, 703-155-155) secondary antibodies for 45 min at 37°C. After washing 6 × 2 min with PBS, coverslips were mounted in elvanol (Tris-HCl, glycerol, polyvinyl

alcohol, and 2% 1, 4-diazabicyclo[2,2,2]octane). Sets of cells were imaged with identical settings on a Zeiss LSM700 microscope with an 40x/1.4 NA objective, a Hamamatsu Orca-Flash4.0 CMOS camera, and custom filters.

For surface expression of Nrxn1 -S5, +S5, and +S5 AAGGL, DIV 3 coverslips were incubated with anti-V5 (mouse IgG2a; 1:5000; Thermo Fisher Scientific, R960-CUS) on the same day as fixation to visualize surface V5-Nrxn1. Neurons were permeabilized the next day and incubated with anti-V5 (rabbit; 1:5000; Cell Signaling Technologies, D3H8Q) for 1 h at 37°C to stain intracellular V5-Nrxn1. Alexa 568-and 647-conjugated secondary antibodies were used to assess surface and intracellular Nrxn1, respectively. For quantification, a mask was generated from the anti-V5 (Alexa 568) signal. Average intensities of YFP, surface V5-Nrxn1 (Alexa 568) and intracellular V5-Nrxn1 (Alexa 647) within this mask was measured using ImageJ (NIH) after subtracting average off-cell background intensities from each channel. Surface V5-Nrxn1 and intracellular V5-Nrxn1 signals were normalized to corresponding YFP signals to account for differences in plasmid expression levels. To combine data from multiple experiments, all measurements were normalized to the mean values of the YFP-P2A-V5-Nrxn1β-S5 group.

For endogenous synapse counts, anti-bassoon (mouse IgG2a; 1:2000; Enzo Life Sciences, ADI-VAM-PS003-F) and anti-PSD-95 (mouse IgG1; 1:500; ThermoFisher, MA1-046) were used to visualize excitatory synapses. Inhibitory synapses were visualized with anti-VGAT (guinea pig; 1:3000; Synaptic Systems, 131 004) and anti-gephyrin (mouse IgG1; 1:300; Synaptic Systems, 147 021). Anti-MAP2 (chicken polyclonal IgY; 1:8000; Abcam, ab5392) was used to label dendrites. For quantification, dendritic regions that appeared to be of good health as assessed using the MAP2 channel were chosen at random. ROIs with pixel overlap between separately thresholded bassoon and PSD-95 channels or VGAT and gephyrin channels were classified as excitatory and inhibitory synapses, respectively. Synapse number is reported per length of MAP2-positive dendrite. To combine data from multiple experiments, all intensity measurements were normalized to the mean values of WT.

Ligand binding assays

For the ligand binding assay, primary neurons were used for appropriate post-translational modification of expressed neurexins. pLL3.7-hSyn-V5-Nrxn1β +S5 or -S5 constructs were transfected into the primary rat hippocampal neurons by nucleofection. At DIV 4, neuron coverslips were incubated with conditioned medium containing the purified NL1-Fc, NL2-Fc, or LRRTM2-Fc proteins for 1 h in the cell culture incubator on an ice pack to inhibit endocytosis. After binding, the coverslips were washed and subject to immunocytochemical procedure without permeabilization. To visualize V5-tagged Nrxn1β, we used anti-V5 (mouse IgG2; 1:5000; ThermoFisher, R960-25). Alexa Fluor 594-conjugated goat anti-human IgG (Fc fragment specific; 1:1000, Jackson Immuno Research; 109-585-008) was used to visualize Fc-tagged proteins. Cells were chosen for imaging based on the expression of transfected construct and a lack of contact with another high-expression cell. For quantification, the surface V5-Nrxn1β positive region was selected for quantifying any encompassing Fc signals within that region. Protein binding signal is reported as a ratio of the integrated intensities of bound Fc-tagged protein to surface V5-Nrxn1β.

Bead induction assays

PLL3.7-hSyn-SEP-V5-Nrx1β -S5 or +S5 or control YFP-MDGA1 constructs were transfected into rat hippocampal neurons by nucleofection. At DIV14, neuron coverslips were incubated with anti-GFP coated beads to cluster the transfected proteins. To prepare anti-GFP coated beads, NeutrAvidin-labeled FluoSpheres (Invitrogen; F-8777; aqueous suspensions containing 1% solids) were rinsed in PBS containing 100 mg/mL BSA (PBS/BSA) then incubated with biotin-conjugated anti-GFP (Rockland Immunochemicals; 600-106-215) at ~6 μg antibody per μl beads in PBS/BSA at RT for 2 h and then rinsed in PBS/BSA. The beads were resuspended in conditioned medium and added dropwise to the neurons on coverslips for 1 h. Neuron coverslips were then put back to their home glia dishes and cultured for 24 h. Immunocytochemical procedures were then performed under permeabilizing conditions.

For imaging, fields were chosen based on expression of the transfected construct and surrounding staining patterns of PSD-95 at endogenous synapses. To assess the presynaptic induction, we used anti-VGluT1 (mouse IgG1; 1:4000; NeuroMab, 75-066), anti-bassoon (mouse IgG2a; 1:2000; Enzo Life Sciences, ADI-VAM-PS003-F) or anti-ELKS (mouse IgG2a; 1:250; Sigma, E4531). To exclude endogenous synapses, we used anti-PSD-95 (mouse IgG2a; 1:500; ThermoFisher, MA1-045) for VGlut1 experiments, and anti-PSD-95 (mouse IgG1; 1:500; ThermoFisher, MA1-046) for bassoon and ELKS experiments. Anti-MAP2 (chicken polyclonal IgY; 1:8000; Abcam, ab5392) was used to label dendrites. Alexa-fluorophore conjugated secondary antibodies generated in goat toward the appropriate species (1:500; Invitrogen; Alexa 568 and Alexa 647 labeled secondary antibodies) were then used to visualize the synaptic proteins. AMCA conjugated anti-chicken IgY (donkey IgG; 1:400) was used to visualize dendrites. Signals of the SEP-Nrxn1β or YFP-MDGA1 clusters at the beads were not amplified by any antibody. Presynaptic inducing activity was measured as mean intensity of punctate VGlut1, bassoon, or ELKS within the area of bead-associated clustered SEP-Nrxn1β or YFP-MDGA1, choosing beads away from MAP2-positive dendrites and excluding any overlap with punctate PSD-95 to exclude native synapses.

RT-PCR and qPCR

Whole mouse brains (three male mice of each genotype at similar ages between 3 and 4 months old) were homogenized and total RNA was extracted with PureLink RNA mini Kit (Thermofisher) as per the manufacturer's protocol. 1 μg total RNA was used for cDNA synthesis with QuantiTect Reverse Transcription Kit (Qiagen). Relative mRNA expression was compared by qPCR using the Applied Biosystems 7300 Real-Time PCR System with Power SYBR 2X mixture (Thermofisher) and the primers listed in Table S2. For ratiometric RT-PCR to assess the fraction of Nrxn1 without the S5 insert, 2 μL cDNA was used with Quick-Load Taq 2X Master Mix (NEB

M0271S), 200 nM forward primer 5′-AGGACATTGACCCCTGTGAG-3′ and 200 nM reverse primer 5′-CACCTACTCTGGTGGGGTTG-3'. To probe PCR efficiency between -S5 and +S5, a mixture of linearized plasmids encoding mouse Nrxn1β(-S5) and (+S5) (500 pg each) was used as PCR template.

DAPI staining for gross brain morphology

Male mice (3–4 months old) were intracardially perfused with 4% PFA in PBS. Brains were rapidly removed and postfixed with the same fixative overnight at 4°C. Sagittal hippocampal slices (100 μm) were prepared using a vibratome (VT1000s, Leica), DAPI stained, and mounted in Vectashield Plus (Vector Laboraties). DAPI images were obtained using a Zeiss ApoTome.2 microscope equipped with a Plan-NeoFluar Z 2.3× objective and stitched using Adobe Photoshop.

Preparation of crude synaptosomal fraction

Brains from 2 to 3 months old female mice were rapidly removed and rinsed with cold PBS. Individual brains were homogenized in 1:10 (weight:volume) buffer A (5 mM HEPES pH 7.4, 1 mM $MgCl_2$, 0.5 mM $CaCl_2$, 1 mM DTT, 320 mM sucrose) supplemented with Protease Inhibitor Cocktail (Roche) in a glass Teflon homogenizer (eight strokes, 1200 rpm). Brain homogenate was centrifuged for 10 min at 1000 x g twice to remove cellular nuclei. The supernatant S1 fraction was centrifuged for 10 min at 12,000 x g, after which pellet P2 was resuspended in buffer B (6 mM Tris pH 8.1, 0.32 M sucrose) supplemented with EDTA-free Protease Inhibitor Cocktail and centrifuged for 15 min at 14,500 x g. This yielded the final pellet, P2′ crude synaptosomal fraction, which was stored at −80°C.

Immunoprecipitation and immunoblotting

Crude synaptosomal fraction samples were incubated with or without 1U/ml each of Heparinase I (Sigma, H2519), II (Sigma, H6512), and III (Sigma, H8891) for two and half hours at 37°C in buffer containing 20 mM Tris-HCl, pH7, 100 mM NaCl, 1.5 mM CaCl2, and EDTA-free Protease Inhibitor Cocktail (Roche). For immunoprecipitation, crude synaptosomal fractions were treated with Heparinases as above and then directly lysed in cold lysis buffer (50 mM Tris-HCl pH 7.4, 150mM NaCl, 1% Triton X-100, 0.03% deoxycholic acid sodium and 1mM EDTA) with Protease Inhibitor Cocktail (Roche) for 30 min on ice. Lysate was centrifuged for 20 min at 21,130 g at 4°C. Supernatant was incubated with anti-Nrxn1 (Synaptic System, 175103) antibodies for 2 h at 4°C. Washed Protein G agarose beads were added to the lysates and the samples rotated overnight at 4°C. After three washes with the heparinase enzyme buffer, the resulting pellets were dissolved in SDS-loading buffer and run on 7.5% polyacrylamide gels. Gels were transferred onto Immobilon P membranes which were blocked in 5% skim milk in Tris-buffered saline/0.025% Tween 20 for 30 min at room temperature followed with anti-Nrxn1 (1:1000; Synaptic System, 175103) antibody in 3% BSA in Tris-buffered saline/0.025% Tween 20 overnight at 4°C. Membranes were further incubated with Clean-Blot IP Detection Reagent (Thermo Scientific) for chemiluminescence before being detected using the SuperSignal West Atto Ultimate Sensitivity Chemiluminescent Substrate (ThermoFisher). Immunoblots were then stripped at 55°C for 15 min, washed three times with Tris-buffered saline/0.025% Tween 20, blocked, and blotted with 3G10 anti-heparan sulfate stub region (1:3000; AMSBIO) at 4°C overnight. Membranes were then incubated with goat anti-mouse HRP conjugated secondary antibodies (Millipore) for chemiluminescence. Immunoblots were then detected using the SuperSignal Chemiluminescent kit (Thermo Scientific).

For direct immunoblotting, synaptosomal fractions were treated with Heparinases and run on a polyacrylamide gel without immunoprecipitation, followed by transfer and blocking as described above. Membranes were incubated with anti-Nrxn1 (1:1000; Synaptic System, 175103) or anti-pan-Nrxn (1:2000; Millipore, ABN161) primary antibodies at 4°C overnight followed by incubation with appropriate HRP conjugated secondary antibodies at room temperature for 1 h. Immunoblots were detected using SuperSignal West Atto Ultimate Sensitivity Chemiluminescent Substrate (ThermoFisher) for Nrxn1 or SuperSignal Chemiluminescent kit (Thermo Scientific) for pan-Nrxn. Subsequent stripping, blocking, re-probing, and detection of anti-tubulin (1:10,000; Millipore, 05–829) were performed as described above. Protein level is reported as a ratio of signal intensities of either Nrxn1 or pan-Nrxn to tubulin, normalized to WT.

Golgi staining and spine counts

P30 brains from female mice were rapidly dissected after isoflurane anesthesia and processed according to instructions provided by the FD Rapid GolgiStain Kit (FD NeuroTechnologies). Sections of 100 μm were used. z stack images of secondary and tertiary dendrites in hippocampal CA1 *stratum radiatum* were collected (optical thickness: 0.5 μm). Spine density and dendrite length were analyzed using a quantification software called 'RECONSTRUCT' (http://synapses.clm.utexas.edu).

Hippocampal slice electrophysiology

For CA1 recordings, brains were rapidly extracted from mice aged P14-P17 and submerged in ice-cold artificial cerebrospinal fluid (ACSF) containing (in mM): 125 NaCl, 2.5 KCl, 2 $CaCl_2$, 2 $MgCl_2$, 1.25 NaH_2PO_4, 26 $NaCO_3$, 25 glucose, pH 7.35 (oxygenated with 95% O_2 and 5% CO_2, 310–320 mOsm). Coronal hippocampal slices (400 μm) were prepared using a vibratome (VT1000s, Leica). Freshly cut slices were placed in a recovery chamber with carbogenated ACSF at 31°C for at least 30 min and then kept at room temperature for 60 min before recording. For CA3 recordings, the brain was rapidly extracted and submerged in ice-cold sucrose-based solution containing (in mM): 87 NaCl, 25 $NaHCO_3$, 2.5 KCl, 1.25 NaH_2PO_4, 7 $MgCl_2$, 0.5 $CaCl_2$, 25 glucose, and 75 sucrose (oxygenated with 95% O_2 and 5% CO_2). Hippocampal slices (400 μm) were cut following[58] and moved to a heated (31°C)

sucrose-based solution containing the same formulation as mentioned above. Slices were allowed to recover for at least 30 min and then kept at room temperature for 60 min before recording.

Slices were transferred to a recording chamber continuously perfused with carbogenated ACSF (2 mL/min). Patch pipettes were pulled from borosilicate glass capillary tubes (World Precision Instruments) using a pipette puller (P-97, Sutter Instruments), with pipette resistances varying between 3 and 6 MΩ. For all whole-cell CA1 recordings except mIPSCs, CA1 pyramidal cells were voltage clamped at −70 mV and the patch pipette solution contained (in mM): $CsMeSO_3$ 130, NaCl 8, $MgCl_2$ 2, HEPES 10, EGTA 0.5, ATP 4, and QX-314 5 (pH 7.2). For CA1 mIPSCs, the patch pipette solution contained (in mM): CsCl 140, CaCl2 0.1, MgCl2 2, HEPES 10, BAPTA 10, ATP 4, and QX314 5 (pH 7.2). CA3 pyramidal cells were voltage clamped at −70 mV and the patch pipette solution contained (in mM): Cs gluconate 122.5, CsCl 17.5, $MgCl_2$ 2, HEPES 10, BAPTA 10, ATP 4, and QX314 5 (pH 7.2). mEPSCs were recorded in the presence of tetrodotoxin (1 μM; Abcam) and bicuculline methiodide (10 μM; Abcam), whereas mIPSCs were recorded in the presence of tetrodotoxin (1 μM; Abcam), CQNX (20 μM; Abcam), and APV (50 μM; Abcam). Evoked EPSCs were recorded in the presence of bicuculline methiodide (10 μM; Abcam). CQNX (20 μM; Abcam) was also added for NMDAR-mediated EPSC input-output curves. All evoked responses were elicited with bipolar tungsten stimulating electrodes (FHC) placed in stratum radiatum of area CA1. For paired pulse ratio recordings (PPR), extracellular field EPSPs (fEPSPs) were recorded with a glass microelectrode filled with ACSF (resistances, 2–3 MΩ). After establishing a stable baseline, responses were set at 40% of maximum and paired pulses were applied while varying the interstimulus interval. Paired pulse ratio is calculated as the ratio of the peak amplitude of the second response over the first response. For evoked whole-cell recordings, the stimulating electrode was placed in stratum radiatum within ∼100–200 μm from the whole-cell patched CA1 pyramidal cell. For input-output curves, cells were held at −70 mV and +40 mV to assess evoked primarily AMPA EPSCs and NMDA EPSCs with 1X stimulation intensity being just below the minimal intensity to elicit both successes and failures. Stimulation was then increased in a multiplicative manner. For responses to stimulus trains, EPSCs were evoked at a low-frequency rate of 0.2 Hz to establish a stable baseline, after which stimulus trains were delivered at a rate of 20 Hz. The last 14 cumulative EPSC points for each genotype were fitted with a linear regression line and back-extrapolated to stimulus number = 0. For AMPA/NMDA ratio recordings, evoked AMPAR-mediated and NMDAR-mediated currents were recorded at −70 mV and +40 mV, respectively. The NMDAR component was analyzed 70 ms after stimulus to ensure that it was free of AMPA receptor contamination. Recordings were low-pass filtered at 2 kHz, and series resistance was left uncompensated except while assessing input-output curves, stimulus trains, and AMPA/NMDA ratios. In those experiments, series resistances were compensated by 40–50%. Cells with changes >20% in series resistance during recording were discarded.

Behavior

Mice for behavior were housed in a reversed 12-h light/dark cycle and assays performed during the dark phase of the cycle to mimic the natural nocturnal behaviors. All behavioral studies were completed with researchers blind to genotype. Generally, the same mice were assessed in all behaviors, although the grooming assay also included some naive mice.

Neurodevelopmental milestones

The neurobehavioral development testing commenced on postnatal day 2 (P2) and was completed on even-numbered days until P24. On each test day, pups were weighed and examined for pinnae detachment and eye opening. The ages at which the pinnae were separated from the head and at which both eyes were first opened were recorded. Pups were tested for a number of reflex responses as outlined below between P2 and P10, and for the auditory startle reflex between P6 and P16.[59–63]

For forelimb and hindlimb grasp reflexes, pups were held up and both the left/right forelimbs or hindlimbs were stroked with slight pressure using a 1 mm diameter copper wire. The age at which stroking caused the stimulated forelimb or hindlimb to grasp the wire (flexion of digits around wire) was recorded.

The crossed extensor reflex, where pinching of one hindlimb causes extension of the opposite hindlimb, is present for the first several days after birth.[61] Pups were held up and the left and right hindlimb were gently pinched between the thumb and forefinger of the experimenter. The age at which contralateral limb extension ceased was recorded.

In the rooting reflex assay to measure tactile reflexes and motor coordination,[63] a cotton swab was slowly brushed from the front to back along the side of the pup's head three times. The age at which the pup responded by orienting its head in the direction of the stimulation was recorded.

To assess the vibrissea reflex, pups were held by the tail and lowered toward a flat surface. Before development of the vibrissae system, the pup's head will make contact with the table, while after development, the pup will respond to vibrissae stimulation by raising its head to avoid hitting the table.[61] The age at which the pup raised its head and extended its forepaws downward was recorded.

To assess the auditory startle reflex, pups were placed on a flat surface and a clicker (70 dB) was sounded next to the pup. Three trials were completed per day and the day at which a startle response (whole body flinch) was observed was recorded.

Novel object recognition

Visual recognition memory was assessed using the novel object recognition test at P22 and P24. Two identical objects (approximately 6 cm × 2 cm x 4 cm) were placed 8 cm from each other in the center of a 25 cm × 25 cm x 30 cm chamber. Beginning at P22, pups were placed in the center of the chamber and allowed to investigate the identical objects for 5 min 1 h later, a second

5-min trial was completed, but with one similarly sized novel object placed 8 cm from the familiar object. The side of the chamber that the novel object was placed was randomly assigned each trial. Trials were recorded with a camera (SX50 HS, Canon) for subsequent analysis. Pups were allowed to investigate both the familiar object and the novel object. The ratio of time spent investigating the novel object and the familiar object was used for statistical analysis.

Ultrasonic vocalization

Observation of ultrasonic vocalizations (USV) began on P1 and occurred on every second day until P15 because this period is when USV emittance is most abundant.[64] For tests, pups were isolated from their mother for 15 min in order to elicit the vocalizations. After the 15-min isolation period, pups were taken one-by-one into the testing room and placed into a glass beaker before going into the recording apparatus (Avisoft-RECORDER USGH UV). Once in the recording apparatus, pups had their vocalizations recorded for 3 min at room temperature with the lights off. USV audio files were analyzed using DeepSqueak software.[54]

Grooming

Mice were tested at 2–3 months of age. Mice were removed from their home cage and placed individually in a recording chamber made entirely of plexiglass and mirrors with an angled mirror under the floor for observing the underside of the mouse. Mice were recorded on a Canon PowerShot digital camera for 1 h in the chamber. Videos were analyzed using the BORIS program.[55] The start and end of each bout of grooming was recorded, with grooming defined as instances of paw licking, nose, face, and head washing, body grooming, leg licking, and tail and genitals grooming.[65] The start and endpoints of grooming bouts were used to calculate the number of grooming bouts, the total grooming duration, and the mean bout duration.

QUANTIFICATION AND STATISTICAL ANALYSIS

Quantification is described in corresponding Method Details sections. Basic statistical information is provided in the figure legends and full statistical details are provided in Table S3. Analysis was performed using GraphPad Prism 8, the statistical program R (www.R-project.org), ImageJ (NIH), and Microsoft Excel. In all cases, data was tested for normality using the D'Agostino and Pearson test. If all datasets passed the test, statistical comparisons were made with Student's unpaired t test or ANOVA followed by post hoc tests for comparisons among multiple groups. Otherwise, nonparametric tests were used. All data are reported as the mean ± standard error of the mean (SEM).